Energy and environmental analysis of a flexible Power-to-X plant based on Reversible Solid Oxide Cells (rSOCs) for an urban district

Energy and environmental analysis of a flexible Power-to-X plant based on Reversible Solid Oxide Cells (rSOCs) for an urban district

Giulio Buffo*, Domenico Ferrero, Massimo Santarelli, Andrea Lanzini

Dipartimento Energia, Politecnico di Torino – C.so Duca degli Abruzzi 24, 10129 Torino (Italy)

*Corresponding author: giulio.buffo@polito.it

ABSTRACT

This study proposes the modeling and the performance assessment of a grid-connected Reversible Solid Oxide Cell (rSOC) plant that is the core system of a polygeneration flexible hub between the national electric grid and the local microgrid of an urban residential district. The system is designed to integrate a thermal storage unit based on phase change material with the rSOC stack by means of heat pipes. At times of low electricity price, the plant produces hydrogen via electrolysis fed preferentially by a dedicated wind farm. Hydrogen is stored as compressed gas and used for the public transportation and electricity production during peak-demand hours. The goal of the study is to investigate the performance and environmental indicators of this novel rSOC configuration and to identify which operating strategy best fits with the analyzed district application. The operating points of the overall system are mapped with a steady-state model and interfaced with thermal storage and loads by a time-resolved dynamic model. The feasible schedules of the system are defined considering the rSOC switching dynamics between fuel cell and electrolysis, and constraints on plant self-sufficiency for both heat and hydrogen vectors. Simulations at different levels of hydrogen demand for mobility (ranging between 10 and 1,000 ton/year) were performed. Results showed an annual efficiency range of 55-70% (including heat to DH) of the polygeneration plant. The environmental analysis showed that the rSOC plant emits 5-50% less CO_2 than the current energy system (gas boilers, grid electricity, diesel buses), when electrolysis is fed by grid-electricity with the present UK carbon intensity in case of wind power shortages.

Keywords: reversible solid oxide cell; polygeneration; hydrogen; power-to-X; dynamic modeling; environmental analysis.

Highlights

- An on-grid rSOC plant with dedicated RES and molten-salt heat storage was modeled
- A time-resolved dynamic model provides self-sufficient schedules of rSOC plant
- Daily global efficiency (H_2+electricity) varies with mobility demand from 51% to 25%

- The system has an annual efficiency of 55-70% (including thermal energy)
- Grid-connected RES-fed rSOC emits 5-50% less CO_2 than a reference energy system

---

List of abbreviations

ASR	Area Specific Resistance	**PCM**	Phase Change Material
BoP	Balance of Plant	**RES**	Renewable Energy Sources
CHP	Combined Heat and Power	**rSOC**	Reversible Solid Oxide Cell
DH	District Heating	**SOEC**	Solid Oxide Electrolytic Cell
EF	Emission Factor	**SOFC**	Solid Oxide Fuel Cell
HSU	Heat Storage Unit	**WD**	Weekdays
OCV	Open Circuit Voltage	**WE**	Weekend days

List of symbols

$\boldsymbol{CF_{SOEC}}$	*%*	Capacity factor of SOEC subsystem
$\boldsymbol{CF_{SOFC}}$	*%*	Capacity factor of SOFC subsystem
$\boldsymbol{E_{BoP,SOEC,d,p}}$	*kWh*	Energy exchanged by the BoP of SOEC subsystem on the d^{th} day (p^{th} schedule)
$\boldsymbol{E_{BoP,SOEC,y}}$	*GWh*	Annual energy exchanged by the BoP of SOEC subsystem
$\boldsymbol{E_{BoP,SOFC,d,p}}$	*kWh*	Energy exchanged by the BoP of SOFC subsystem on the d^{th} day (p^{th} schedule)
$\boldsymbol{E_{BoP,SOFC,y}}$	*kWh*	Annual energy exchanged by the BoP of SOFC subsystem
$\boldsymbol{E_{DH,d}}$	*MWh*	Energy supplied to the DH scheme on the d^{th} typical day
$\boldsymbol{E_{DH,y}}$	*GWh*	Annual energy supplied to the DH scheme
$\boldsymbol{E_{load,y}}$	*GWh*	Annual electric energy supplied to the residential district
$\boldsymbol{E_{SOEC,d,p}}$	*kWh*	Electric energy consumed in SOEC mode on the d^{th} day (p^{th} schedule)
$\boldsymbol{E_{SOEC,grid,y}}$	*GWh*	Annual electric energy purchased from the grid to feed electrolysis
$\boldsymbol{E_{SOEC,wind,y}}$	*GWh*	Annual electric energy from wind power plant to feed electrolysis
$\boldsymbol{E_{SOEC,y}}$	*GWh*	Annual electric energy to feed electrolysis
$\boldsymbol{E_{SOFC,d,p}}$	*kWh*	Electric energy produced in SOFC mode on the d^{th} day (p^{th} schedule)
$\boldsymbol{E_{SOFC,load,y}}$	*GWh*	Annual electric energy supplied to the residential district by SOFC
$\boldsymbol{E_{wind,SOEC,y}}$	*GWh*	Annual energy supplied by the wind power plant to the SOEC
$\boldsymbol{E_{wind,grid,y}}$	*GWh*	Annual energy supplied by the wind power plant to the grid

$E_{wind,load,y}$	*GWh*	Annual energy supplied by the wind power plant to the residential loads
$E_{wind,y}$	*GWh*	Total annual production of the wind power plant
$h_{SOFC,y}$	*h*	Hours of SOFC operation during the year
$h_{wind,grid,y}$	*h*	Hours during the year with surplus power from wind plant supplied to the grid
$H_{2,mob,d}$	*kg*	Daily demand of mobility hydrogen on the d^{th} day
$H_{2,mob,y}$	*ton*	Annual demand of mobility hydrogen
k	-	Shape factor
L_d	*km*	Daily distance travelled by the bus fleet
L_y	*km*	Annual distance travelled by the buses
LHV_{H_2}	*MJ/kg*	Lower heating value of hydrogen
N_h	-	Number of houses served by the DH scheme
P_{H_2}	*MW*	Chemical power of the H_2 outlet (SOEC) /inlet (SOFC) stream
$\widehat{P}_{wind,grid,y}$	*MW*	Peak of surplus wind power directly supplied to the grid during the year
Q_{BoP}	*MW*	Heat exchanged by the BoP
Q_{stack}	*MW*	Heat exchanged by the stack
W_{BoP}	*MW*	Power for/from the operation of BoP of the rSOC plant
$W_{stack,AC}$	*MW*	Alternating current input/output (SOEC/SOFC) power
$W_{stack,DC}$	*MW*	Direct current input/output (SOEC/SOFC) power
x	*m/s*	Wind speed
z	*m*	Height

Greek symbols

α	-	Wind shear coefficient
β	*m/s*	Scale factor
$\eta_{CHP,SOEC}$	*%*	CHP efficiency of the stack in steady-state SOEC mode
$\eta_{CHP,SOFC}$	*%*	CHP efficiency of the stack in steady-state SOFC mode
$\eta_{EL,SOEC}$	*%*	Electric efficiency of the stack in steady-state SOEC mode
$\eta_{EL,SOFC}$	*%*	Electric efficiency of the stack in steady-state SOFC mode
$\eta_{d,p}$	*%*	Daily electric efficiency of the system on the d^{th} day (p^{th} schedule)
$\eta^*_{d,p}$	*%*	Daily global efficiency of the system on the d^{th} day (p^{th} schedule)
η^*_y	*%*	Annual global efficiency of the system

1. Introduction

The transition to the availability of clean and affordable energy to achieve the 7th world Sustainable Development Goal (SDG) can involve different measures [1], such as the use of renewable energy sources (RES). However, the penetration of RES in the electricity production portfolio is currently limited by the randomness of their availability. Several strategies are currently being pursued to increase the flexibility of electricity grids with respect to RES: some of these strategies follow the so-called "Power-to-X" scheme, in which electricity is not only stored for time-shifted power delivery, but also employed to cover non-electric demand in different sectors, such as transportation, heating and industry [2]. Electricity can be converted into many "X" energy vectors. Hydrogen is a very flexible, zero emissions energy vector with potential use in several applications, either as it is or as a platform molecule [3]. In fact, hydrogen can be efficiently generated by water electrolysis and then reconverted to electricity in fuel cells (or even in thermal machines, with lower efficiencies), used in CHP systems to produce heat, or it can be directly used in fuel cell electric vehicles (or even blended with natural gas to feed traditional gas engines) for mobility applications [4]. Hydrogen can also be injected into the existing natural gas grid to some extent [5], or used as a commodity (or reactant) in industrial sectors (e.g., steel-making plants or ammonia plants).

Several technological schemes can be adopted for a hydrogen-based polygeneration concept: one of these is the Reversible Solid Oxide Cell (rSOC). rSOCs are promising electrochemical devices for electricity conversion and storage in the form of hydrogen (or, in some schemes, in form of a syngas blend of H_2 and CO), fulfilling both electrolysis and fuel cell requirements in a single component [6]. If coupled with an adequate system of flexible energy storages, the rSOC polygeneration plant can both absorb power peaks (electrolysis) from input RES and provide electricity and heat (fuel cell) to users, thus helping the mitigation of power fluctuations on the electric grid on the supply side and at the same time providing several energy commodities as output.

Literature reports an increasing interest on rSOCs in recent years, with several works focusing on the application of this technology to energy storage and polygeneration systems [7]–[16] and some with a focus on their self-sufficient and repeatable operation [17]–[20]. Several projects are currently dealing with rSOCs at large scale. For instance, in the US for the demonstration of an rSOC system for a microgrid environment [21], the excess power generated in off-peak hours by RES is exploited to produce H_2 by electrolysis: the stored H_2 is used in fuel cell mode to provide power during peak electricity demand hours.

The present work assesses the dynamic operation (i.e., SOEC/SOFC switch) of an rSOC-based polygeneration system designed as interface between the electricity distribution grid, a wind power station and a district microgrid. The polygeneration system allows thus for cross-sector decarbonization of a local energy system via hydrogen carrier. The plant's performance was simulated based on realistic profiles of domestic thermal and electricity loads and public mobility demand in a typical urban district located in the UK. The priority task of the plant was to

produce hydrogen for local public mobility using electricity from a dedicated wind power station integrated in the system, with the goal of replacing an existing diesel-based bus fleet. The microgrid loads were powered primarily by wind power. The plant also served the microgrid loads by running the SOFC during peak-demand hours in case of insufficient wind power generation. A compressed-gas storage ensured the daily hydrogen self-sufficiency of the plant, as imposed by the operating logic. A heat storage unit was designed primarily to ensure the thermal self-sufficiency of the plant. The residual heat in the thermal storage was provided to a local District Heating (DH) network.

To the authors' knowledge, a polygeneration system providing hydrogen for local mobility, grid services, electricity and heating by integrating local RES generation is a novel application for rSOCs. Moreover, even though the SOC integration with a PCM-based storage [22], [23] and heat pipes [24]–[27] has been already studied, the integration of both of them including thermal recovery for DH represents a novel plant configuration. The goal of the study is to investigate this novel rSOC configuration by performance and environmental indicators and to identify which operating strategy best fit with the analyzed district application.

To this purpose, the energy and environmental performances of the polygeneration system were assessed for different levels of the hydrogen mobility demand (from 9.77 to 976.5 ton/year, corresponding to a traveled distance of 100,000 and 10,000,000 km/year respectively) in all the feasible operating schedules of the plant, keeping the size of the Power-to-X system constant. In particular, the variation of daily electric efficiency and global efficiency during the year and the overall annual efficiency were evaluated to analyze the energy performance. The CO_2 emissions of the polygeneration system were evaluated with respect to the reference energy scenario, in which electric, thermal and mobility demands are covered by grid electricity, gas boilers and diesel buses. Finally, the positive impact on the distribution grids in terms of power peak reduction is highlighted.

In the paper, the layout of the proposed rSOC-based Power-to-X system is presented in Section 2. Section 3 focuses on data sources of the demand of different energy vectors, steady-state and dynamic modeling of the plant and the methodology for the performance assessment. The Results section shows and discusses the outcome of the simulations performed, the efficiency and the environmental benefits of the proposed system. Details of the economic analysis are beyond the scope of the current study and will be covered in future.

2. Concept of the rSOC-based Power-to-X plant

This section presents the conceptual layout of the proposed rSOC system (Figure 1). The plant interfaces with:

- the hydrogen demand of the H_2-fed bus fleet;

- the wind farm power input, which foremost covers the local district loads and, on top of that, the electrolysis;
- the electricity demand of the local microgrid, fed during peak-demand hours;
- the electric grid, from which the system imports electricity in case of insufficient wind production to cover the power demand for electrolysis and, in case, the local district loads;
- the thermal loads of a District Heating scheme.

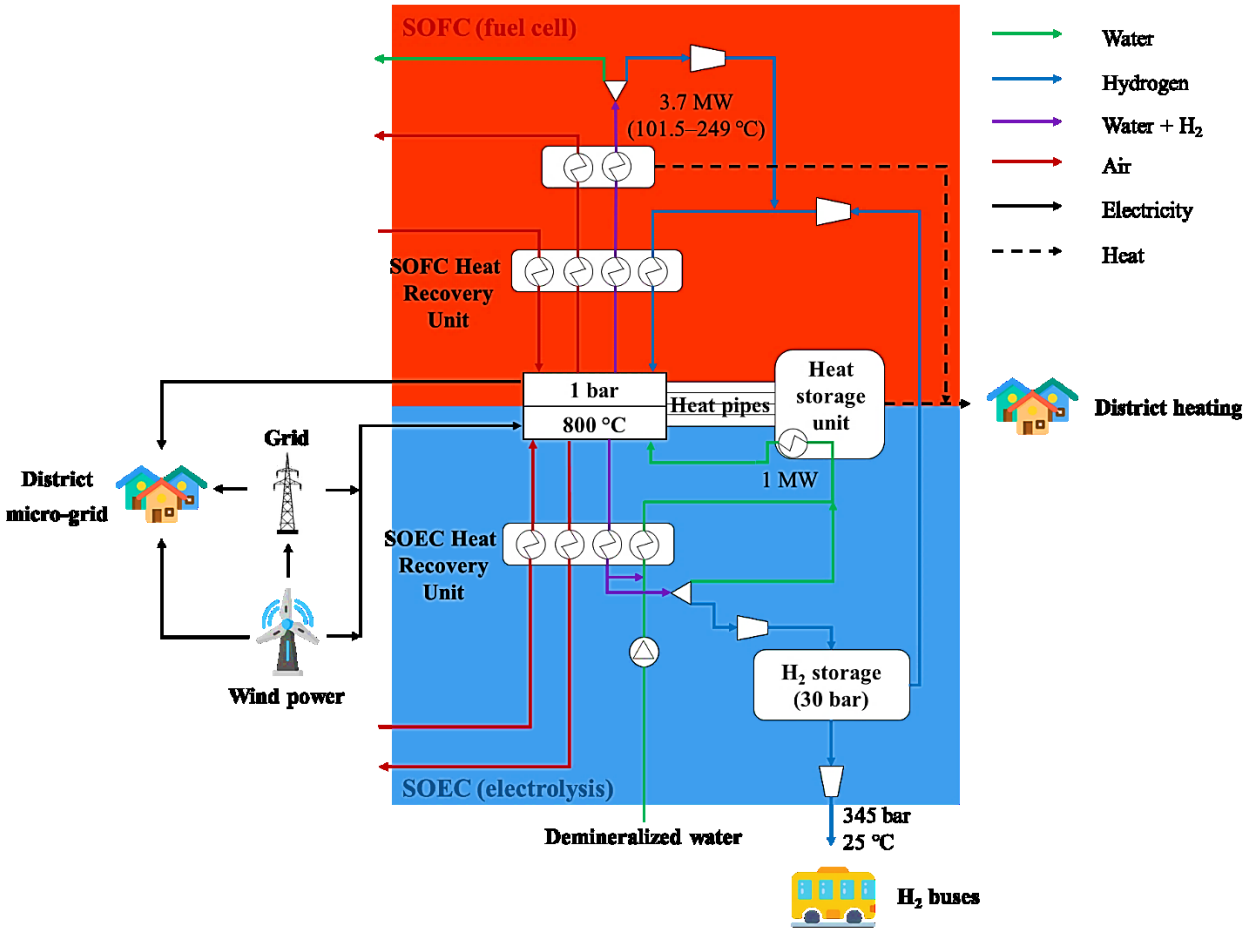

Figure 1 - Conceptual scheme of the rSOC-based Power-to-X system

The core section of the system is the reversible SOFC/SOEC stack unit. The nominal size of the SOFC system has been arbitrarily set equal to 10 MW_e, which can fit with the peak demand of a mid-size residential district (i.e, 27,000 inhabitants). The SOEC/SOFC nominal power ratio is assumed equal to 5, which is close to the value for the optimization of the stack thermal management [28]. So, the nominal SOEC power is 50 MW_e. To reach the total nominal power of the system, several modules of stacks are needed with the current size of the SOC technology. In the simulations it is assumed that the control strategy is the same for all the modules installed in

the rSOC plant: thus, at a given time the operating point is the same for all the cells of the system. For this reason, when considering all the cells of the system, in the following we will simply refer to as stack.

Both SOFC and SOEC operations are performed at ambient pressure of 1 bar and use air as oxidant during SOFC operation and as sweep gas for the SOEC. The hydrogen produced in SOEC is compressed to 30 bar and delivered to a storage unit: this pressure has been chosen as reasonable hydrogen pre-compression level before a multi-stage compression to higher pressures. Stored H_2 is either fed to the SOFC through a turbo-expander or to the bus refilling station at 345 bar (i.e., 5,000 psi) by a multi-stage compression.

A Heat Storage Unit (HSU) based on molten salt is included in the system for combined thermal management of the stack, steam production and preheating in SOEC mode and thermal buffering of the heating output to a DH network. Sufficient waste heat from SOFC operation has to be provided and stored in HSU to run electrolysis without the need for additional energy for steam generation. The operating temperature chosen for the stack depends on the melting point of the salt used in the buffering HSU [29]. Sodium chloride was selected as salt for the HSU, which has a melting temperature of 800 °C at ambient pressure [29] that is compatible with the SOC operation. This choice is expected to make the thermal storage also economically viable with respect to using more complex thermal storage materials. A system of sodium planar heat pipes [24], [25], [27] performs the mutual exchange of heat between the cell stack and the HSU. The operation of these devices can be assumed isothermal if the heat duty does not exceed 740 W per heat pipe (axial heat transfer density of over 100 W cm^{-2}) [25], hence allowing a single heat pipe interconnector to cool several cell layers of the rSOC stack, as the maximum heat flow produced and exchanged by the single cell resulted to be about 180 W in the simulations performed.

3. Methodology and case study

This section of the paper describes the methodology developed to get the performance map of steady-state operating points (Section 3.3), which will be interfaced with the wind power station (Section 3.2) and the loads of the residential district (Section 3.1) by the dynamic simulation model (Section 3.4). The performance indicators are described in Section 3.5.

3.1. Demand side

The different energy vectors leaving the rSOC module represent the energy mix of the polygeneration system. The elements of this mix are distributed by different infrastructures that interact with the rSOC plant.

3.1.1. Electric demand

An accurate knowledge of the household loads is important when distributed energy technologies have to be sized into the local network [30]. A major issue in modelling the electric load of residential buildings is reproducing the variability among dwellings due to the random use of different electric equipment: in that sense, a stochastic model to obtain load profiles of household electricity has to be developed necessarily [31].

For this case study, a Monte Carlo bottom-up stochastic model was developed taking the cue from the model adjusted for English East Midlands by Richardson et al. [32], [33] to generate 24 electric demand profiles of the district with time step of 1 minute, distinguishing between weekdays and weekend days in the 12 months. The availability of the input transition probability matrices [32] for the model allowed to simulate the active occupancy of each dwelling through a Markov chain. Besides this data, the model required:

- household size data (i.e., the number of occupants) [32];
- saturation level and technical data of the electric household appliances (including lighting) [32], [33];
- 10-min-resolved activity profiles [32];
- outdoor irradiance levels, simulated using PVGIS [34].

The model identified that 11,612 households (about 27,000 people) have a cumulated peak load of 10 MW_e, corresponding to the nominal size of the SOFC.

3.1.2. Hydrogen reference demand

In this study, the hydrogen produced by electrolysis and stored at 30 bar can be further compressed in a refueling station serving a fleet of buses of the public transport service. The fuel consumption for mobility hydrogen was assumed to be 9 kg_{H2}/100 km, according to FCH JU [35]. The demand of H_2 for public transportation buses is presented in Table 1, distinguishing between weekdays and weekend days during summertime (from June to August) and the remaining months of the year. A 10%-excess of hydrogen is considered to ensure the return of buses to depot and for any emergency. In order to estimate the annual travelled distance for a public bus route serving a urban district in UK, a route (in both outbound and inbound directions) operated in the city of Leicester (UK) was considered [36]. A travel distance of about 1 million km/y, corresponding to 89 ton_{H2}/y, was estimated.

Table 1 - Reference demand of mobility hydrogen

	Period from September to May		**Period from June to August**	
	Weekdays	**Weekend days**	**Weekdays**	**Weekend days**
L_d **(km)**	3,544	2,102	1,581	1,032

$H_{2,mob,d}$ (kg)	350.86	208.12	156.46	102.19

3.1.3. Thermal reference demand

For the thermal demand of the district, it was assumed that heat is supplied to users through a DH scheme with 120/90 °C supply/return temperature and thermal losses equal to 5%. During the heating season (from 1st October to 30th April), DH operates with the following schedule:

- from 6 a.m. to midnight on weekdays;
- from midnight to 2 a.m. and from 6 a.m. to midnight on weekend days.

For the simulation of the thermal loads, the thermal module of the stochastic model proposed by McKenna and Thomson [37] was adopted.

3.2. Wind power generation

On the supply side, the rSOC system can promote the introduction of distributed renewable power plants in the energy generation portfolio by softening the impact of their intermittent productivity on the electricity grid. Among the intermittent RES, solar irradiance clearly features an extreme variability throughout the day that may not match with the SOEC/SOFC scheduling imposed instead by both the distribution of demand peak and off-peak hours and the self-sufficiency constraints of the proposed system (Section 3.4.1). Hence considering the logic adopted for the rSOC dynamic operation (Section 3.4.1), the proposed system was assumed to be coupled with a wind farm.

Combined with the rSOC-based system, the wind farm can serve primarily the local loads, then the SOEC operation for hydrogen production and, in case, provide a power input to the grid, if surplus power is still available. In this way, rSOC system can provide a grid service by reducing RES power peaks on the grid, thus helping to maintain the power quality on the grid. In fact, feeding intermittent power into an electricity grid can affect power quality, with an impact (e.g., flickers, brownouts) depending on the degree to which the intermittent source contributes to the instantaneous load [38]. On the other hand, when the RES power is not sufficient to supply local loads, the stored hydrogen can be reconverted to electricity by SOFC. In this way, the rSOC-renewable combination on local microgrid provides flattened input/output power profiles to the electricity grid.

The wind source is well distributed over the day even if characterized by continuous fluctuations. The productivity of a wind turbine depends on the specifications of the machine and on the windspeed getting to the rotor. Windspeed is the source of stochasticity in the prediction of the power output and follows the Weibull distribution:

$$f(x) = \frac{k}{\beta}\left(\frac{x}{\beta}\right)^{k-1} exp\left[-\left(\frac{x}{\beta}\right)^{k}\right] \quad \text{Eq. (1)}$$

where k and β are the shape and scale factors, respectively, and depend on the geographical location and landscape conditions of the installation site.

A Monte Carlo simulation was used to generate a 1-minute-resolved average windspeed profile for each season starting from the characteristic parameters of a weather station in UK, using data from the surroundings of the city of Nottingham, in English East Midlands (53° N, 1.15° W) presented in the Table 2 [39].

Supposing that the anemometer in the considered station is at the standard height z_1 = 10 m, the profile of windspeed x_2 at the height of the wind turbine hub (z_2 = 75 m) was determined assuming conservatively a wind shear coefficient α = 0.143 (neutral stability conditions of the atmosphere) [40]:

$$x_2 = x_1\left(\frac{z_2}{z_1}\right)^{\alpha} \quad \text{Eq. (2)}$$

where x_1 is each of the elements of the four windspeed profiles generated by the Monte Carlo model.

Table 2 - Characteristic parameters for the observational site in Nottingham. Source: [39]

	Average wind speed ($\bar{x}$, m/s)	**Shape factor (k)**	**Scale factor (β, m/s)**
Winter	5.51	2.3	6.225
Spring	5.145	2.61	5.798
Summer	4.261	2.76	4.790
Autumn	4.729	2.3	5.351

Ten 1.5-MW power turbines were assumed to operate in the system. The power output profile was soundly determined considering an efficiency equal to 40% and cut-in, rated output and cut-out speeds equal to 3, 11 and 25 m/s, respectively. The total installed capacity has the same order of magnitude of the electric loads of the residential district (average demand of 5.85 MW with a peak of 10 MW) in order to restrict the size (and, hence, the investment cost) of the wind farm and to limit the share of excess wind power that must be absorbed by the electric grid. Thus, the size of the wind farm was set following the abovementioned criteria, without performing a size optimization based on plant performance or environmental indicators, which is out of the scope of this work.

3.3. Steady-state model of the plant

The mass and energy balances of the whole plant and the thermodynamic transformations of the operating streams were simulated using the commercial process simulator Aspen Plus™. A model for each of the two sections represented in Figure 1 was developed.

The modeling approach followed for the thermo-electrochemical simulation of the SOC system is a lumped stack volume [41]. It simulates the shift of the operating point of the cells along the polarization curve, which is assumed with an exclusively ohmic behavior:

$$V_c\,(i) = OCV - ASR\,i \qquad \text{Eq. (3)}$$

The parameters of the cells that are kept constant in all the models are the size of the cells (22x22 cm^2), the Area Specific Resistance (ASR = 0.241 Ω*cm^2) [41] and the Open Circuit Voltage (OCV = 0.952 V, calculated).

The other components of the Balance of Plant (BoP) are: water pumps, heat exchangers for reactants pre-heating, steam generation and products cooling, hydrogen compressors to reach the storage pressure (in SOEC) and a turboexpander between the hydrogen storage and the fuel cell (in SOFC). The operation of the BoP is defined by the following specifications:

- Efficiency of isentropic compressors: 72%.
- Efficiency of hydraulic pumps: 54%.
- Efficiency of isentropic turboexpander: 71%.
- Pressure drop in heat exchangers: 0.05 bar.
- Efficiency of the inverter: 90%.

The detailed description of the models for SOEC and SOFC subsystems is provided in the supplementary material.

The total efficiencies of SOFC and SOEC stacks (i.e., not including the BoP) are calculated with Eq. (4) in SOFC mode considering a fuel utilization of 90% and with Eq. (5) in SOEC, taking into account the DC/AC conversion:

$$\eta_{CHP,SOFC} = \frac{W_{stack,DC} + Q_{stack}}{P_{H_2}} \qquad \text{Eq. (4)}$$

$$\eta_{CHP,SOEC} = \frac{P_{H_2} + Q_{stack}}{W_{stack,DC}} \qquad \text{Eq. (5)}$$

According to the efficiency definitions given above, Q_{stack} is the heat flow exchanged by the stack through the heat pipes, which has positive sign in case of exothermic stack operation.

The process streams can be coupled in a network of heat exchangers in such a way that thermal power released by streams that cool down is provided coherently to other streams that require heating: the pinch analysis methodology seeks to minimize the overall external thermal supply or removal. The pinch analysis was applied for SOFC and SOEC subsystems separately, since the two systems cannot operate simultaneously.

The thermal module in dynamic model (Section 3.4.2) employs the results for the system thermal management.

3.4. *Time-resolved dynamic model of the system*

A MATLAB™ time-resolved model interfaces the map of steady-state operating points of the rSOC system (shown in Table 3 in the Results section) with the temporal profiles of energy demand of the residential district (Section 3.1) and wind power generation (Section 3.2).

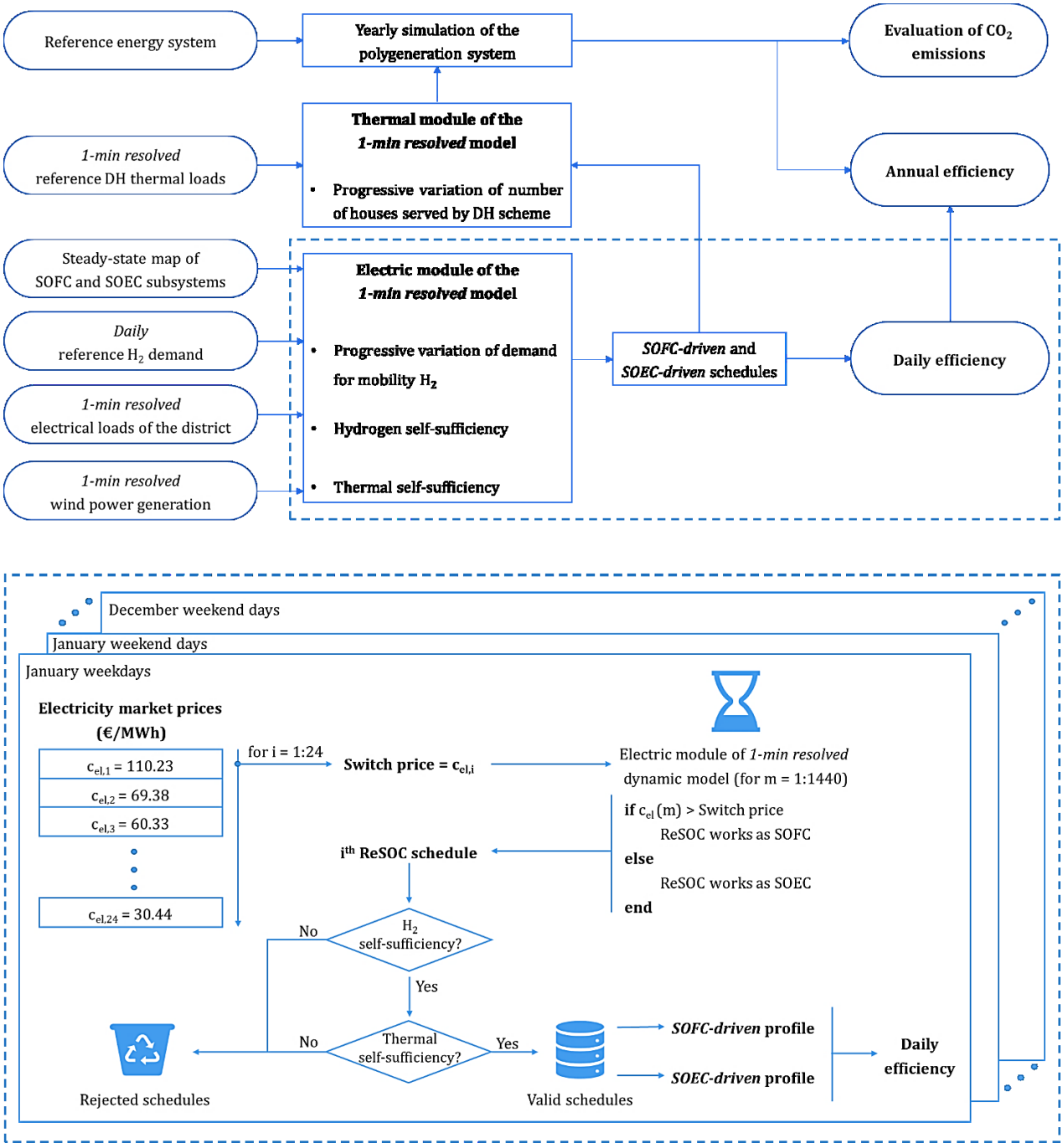

Figure 2 - Workflow of the dynamic model (top panel) with a detail of the electric module (bottom panel)

It relies on two consecutive steps defining the dynamic operation of the rSOC plant (i.e., scheduling the SOFC/SOEC dynamic switch) and, on top of that, the management of thermal demands of the polygeneration system (Figure 2).

3.4.1. Dynamic operation of the rSOC plant

The operation strategy of a polygeneration plant depends on (i) the level of priority that is assigned to each output commodity (i.e., the priority of dispatch of each energy product, provided that the throughput of single products cannot be modulated independently from the others), (ii) the time-profile of the demands and (iii) the technological constraints of the plant, which cannot allow it to always follow the demand profiles of the commodities.

For the rSOC plant analyzed in this study, the output commodities are hydrogen, electricity and heat for DH. The demand profile of hydrogen is given on a daily basis (see Section 3.1.2), while electricity and thermal demands have time-dependent profiles with 1-minute resolution (see Section 3.1.1 and 3.1.3).

Priority has been given to the production of hydrogen (SOEC mode) for the daily mobility demand. Hence, every day the rSOC plant must provide the hydrogen required by the mobility demand. In the time-resolved dynamic model, this first-level priority is enforced as part of the hydrogen self-sufficiency constraint on a daily scale: the hydrogen produced during SOEC operation covers not only the amount of hydrogen delivered to the bus refueling station but also the amount of hydrogen consumed by the SOFC during each day. Imposing a daily hydrogen self-sufficiency constraint allows to have a hydrogen tank sized for one-day operation, which is a reasonable assumption for a plant located in an urban district, where it is likely that only a limited amount of hydrogen can be stored for space availability and safety reasons. Furthermore, a hydrogen tank with a daily (or, at most, weekly) charge/discharge frequency has installation and maintenance costs that are much lower than in case of a seasonal storage. A year-through self-sustaining hydrogen tank fits well in an off-grid system fed by RES with a high variability throughout the year [18]; the studied system, instead, fully exploits the RES availability and the connection to the electric grid avoids both hydrogen shortage and surplus in the storage unit, ensuring the level of hydrogen necessary for the conversion into the X energy carriers demanded in every moment of the year.

The second level of priority is given to the electricity generation (SOFC mode) for the local microgrid in the hours of peak demand on the electricity distribution grid, identified by the electricity price (i.e., hours with the higher electricity price).

The thermal energy to DH has the lowest level of priority. In fact, the heat storage HSU is designed primarily to ensure the thermal self-sufficiency of the plant: only a fraction of the recovered heat is provided to DH. The heat

stored in the HSU during SOFC operation (and in exothermic SOEC) must be sufficient to sustain the endothermic electrolysis of water and to produce and pre-heat steam feeding the SOEC stack (Section 3.3), on a daily basis.

Regarding the operational limits, the SOC stack can operate in either fuel cell/electrolysis mode between 0% and 100% of the nominal power, with a constraint on the rate of change of the power output/supply (± 10% of nominal power) during transients. This constraint can have an impact only on matching the electricity demand profile, as an electricity storage is not included. The power-rate constraint takes into account all the thermal and fluidic transients occurring in the stack that the steady-state thermodynamic-electrochemical rSOC performance map and the dynamic model are not able to simulate. Limiting the power variation rate of the stack is thus a way to include transient limitations in the simulation. It is worth noting that we are assuming to maintain the rSOC always in operation in electrolysis or fuel cell mode and we are not including rSOC switch-on/off transients (e.g., for maintenance or failures).

Starting from the input profiles of electric loads, wind and hydrogen and following the abovementioned priority levels and SOC operational limits, the dynamic model first calculates the daily rSOC operational profiles, as shown in Figure 2.

The dynamic model calculates the schedules of operation of the plant for each of the 24 typical days – each week- and weekend day of the 12 months – with a time-step of 1 minute by assigning the operating mode and power level of the stack (i.e., kW in SOEC or SOFC mode). As the performance map of the stack is fixed, a given power level corresponds to a precise current-voltage point and efficiency of the stack. In order to calculate each schedule, the model imposes at first the fuel cell (SOFC) operation in the hour(s) of the day in which the electricity price [42] is higher. This choice is driven by the goal of the plant to provide electricity to the microgrid preferentially in the hours of higher demand to the distribution grid, which have been identified using the electricity price as indicator of the peak-demand hours. The model first calculates the actual load profile that the SOFC has to provide, which is the difference between microgrid load and wind power generation. In fact, the electric demand of the microgrid is fulfilled first by wind power generation and then by the SOFC. Then, the dynamic model modifies minute by minute the SOFC power level in the assigned time slots in order to provide this actual load by adopting a load-following logic. The hydrogen demand of the SOFC operation is immediately calculated from the stack current, given by its performance map (Table 3 in Results section).

During the peak-demand minutes, the wind generation could be higher than the electricity demand and the actual load requested to the SOFC would be negative. In this case, the surplus wind production is provided to the distribution grid, while the SOFC is set in hot-standby at zero power, thus not switching to electrolysis to avoid many short transients.

Once the SOFC hours are assigned for every schedule, also the SOEC hours of the day are fixed, as they cover the remaining hours of the day. The model calculates the 1-minute resolved SOEC power profile, considering the wind

power output exceeding the electric load of the microgrid as the first source for water electrolysis. If the wind power surplus is not sufficiently high to satisfy the H_2 self-sufficiency constraint, the model computes the constant power rate that should be imported from the electric grid in SOEC hours to this aim: this rate is kept constant during the SOEC hours of every day in order to limit the grid disturbances due to fluctuating power request. The choice of feeding electrolysis during off-peak hours also allows to reduce the cost of electricity imported for SOEC operation. If wind power production is even less than the district demand, both SOEC demand and part of the electric loads of the microgrid are necessarily covered by grid electricity.

Following this logic, the electric module of the dynamic model calculates the SOFC/SOEC 1-minute-resolved schedules of the plant for each of the 24 typical days – each week- and weekend day of the 12 months –.

3.4.2. Thermal management of the system

Heat is a crucial point in the management of the plant from a double point of view:

- at the plant side (that means, heat management inside the plant itself), one should consider the variable and, sometimes, conflicting thermal behaviors of rSOC plant according to the operating mode;
- at demand side, it is necessary to take into account the large variability of heat demanded by end-users not only on a yearly scale, but also during the same day.

Since thermal demand and supply do not always match, a high-T molten-NaCl buffer shifting heat stored at 800°C in time was included into the plant to minimize the amount of wasted heat. It is worth noting that such a thermal storage integrated with the SOC stack by heat-pipes is technically a very complex solution, but it allows the recovery of high-temperature heat for the autonomous stack operation, which otherwise would need external heat sources with great drawbacks on the system in terms of energy and environmental performance.

Besides the in/out heat fluxes due to the rSOC operations determined by the electric module of the dynamic model, the HSU satisfies also the heat demand of the DH scheme (including 5% losses). The thermal module of the dynamic model determines the 1-min-resolved yearly profile of the HSU. It also estimates the number of houses in the DH scheme requiring the residual heat in the HSU that exceeds the amount necessary to fulfill 100% of the thermal demand of the plant itself. In other words, all the heat stored in HSU exceeding the heat demand of the plant is delivered to the DH. In this way, the yearly energy balance on the HSU is satisfied and the heat necessary to feed the internal and external applications is available in every moment of the year-through simulation.

3.5. Assessment of the system performance

Different technical and environmental indicators of the polygeneration system were evaluated along one year of operation, considering the variation of the polygeneration mix. The penetration of hydrogen mobility is varied parametrically between 9.77 to 976.5 ton/year (i.e., from 0.1 up to 10 times the reference demand defined in Table 1), while the electric load profile of the residential district and the wind power generated are the same for all the dynamic simulations.

3.5.1. Daily efficiency

The steady-state efficiency indicators (Eqs. 4 and 5) do not take into account the cyclic schedules of the rSOC plant. The indicator that most effectively represents the performance of such a system is the so-called roundtrip efficiency, provided that the energy stored in the hydrogen carrier is converted back only to the original form (electric power). Indeed, as the system is producing several commodities and is simulated on 24 typical days throughout one year, it is possible to define different types of daily efficiency.

The daily electric efficiency is defined as the ratio of the net electric energy produced in SOFC mode to the total electric energy consumed in SOEC mode [14], recalling that energy has positive sign if it flows from the rSOC system towards the environment:

$$\eta_{d,p} = \frac{E_{SOFC,d,p} + E_{BOP,SOFC,d,p}}{\left|E_{SOEC,d,p} + E_{BOP,SOEC,d,p}\right|} \qquad \text{Eq. (6)}$$

It is also interesting to evaluate the daily global efficiency of the polygeneration system, which reasonably also takes into account the produced hydrogen for mobility as a useful outcome of electrolysis (E_{SOEC}):

$$\eta^{*}_{d,p} = \frac{E_{SOFC,d,p} + E_{BOP,SOFC,d,p}}{\left|E_{SOEC,d,p} + E_{BOP,SOEC,d,p}\right|} + \frac{H_{2,mob,d} \cdot LHV_{H_2}}{\left|E_{SOEC,d,p} + E_{BOP,SOEC,d,p}\right|} \qquad \text{Eq. (7)}$$

Being LHV_{H2} (120 MJ/kg) the lower heating value of hydrogen.

Since the daily efficiencies depend on the operating conditions of the rSOC plant, these performance indicators were computed for the different schedules of the 24 typical days, at each run corresponding to a given penetration of H_2-fed mobility.

3.5.2. Annual efficiency

The thermal module of the model evaluated the annual heat balance of the system on the HSU (Section 3.4.2). Thermal energy has not been considered to compute the daily global efficiency, because the thermal self-sufficiency regards the excess and deficit of heat only inside the boundaries of the rSOC stack (Section 3.4.1). In fact, the balance of the whole polygeneration system including DH scheme is closed on an annual scale, rather than daily, thanks to the presence of the HSU, which also acts as a seasonal storage. Hence, as a final performance index of the modeled polygeneration system, one can compute the value of the annual efficiency as:

$$\eta_y^* = \frac{\left(E_{SOFC,load,y} + E_{BOP,SOFC,y}\right) + H_{2,mob,y} \cdot LHV_{H_2} + E_{DH,y}}{\left|E_{SOEC,y} + E_{BOP,SOEC,y}\right|} \qquad \text{Eq. (8)}$$

with all the energy contributions evaluated on a yearly scale.

3.5.3. CO_2 emissions

An important indicator of the performance of a polygeneration system from the environmental point of view is the amount of carbon dioxide emitted during its operation. Indeed, even though the rSOC has zero direct CO_2 emissions, the electrolyzer is partially fed with grid-electricity, which is not completely renewable and has a non-zero CO_2 intensity. Thus, the indirect emissions deriving from the use of grid electricity could overcome the advantages of eliminating diesel and gas boilers emissions. To evaluate the environmental performance of the polygeneration plant with an alternative case, a reference energy system is set, which provides the same commodities (i.e., fixing the demand of electricity, heat and mobility). The emissions of the rSOC plant were thus compared with those of the reference system.

The reference energy system completely relies on electric grid for the match of electricity demand, distributed gas boilers with 85-100% LHV-based efficiency for covering thermal loads and Euro 3 Diesel-fueled buses for public transport. Although Euro 3 standards are dated back to year 2000, 28% of buses in European Union were still Euro 3 in 2015 and almost 22% were Euro 2 and older [43]: in fact, the renewal of an entire bus fleet is usually achieved over a bus lifecycle (12 years). So, considering a fleet of Euro 3 Diesel buses is representative of a reference public transport system in EU. Each item of the demand side is associated to its average emission factor (EF):

- grid electricity is supposed to have an average carbon intensity of 381.46 g_{CO2}/kWh [44];
- gas boilers have an EF of 2.03 kg_{CO2}/Nm^3 of natural gas [44], assuming a higher heating value equal to 39.73 MJ/Nm^3;

- the emissions of Diesel buses vary according to the covered distance and depend on several factors (such as occupancy, road type); an average value of 1,152.31 g_{CO2}/km was taken from Ref. [44].

4. Results and discussion

In order to assess the feasibility of the Power-to-X polygeneration and storage system based on rSOCs and evaluate its energy and environmental performances, we simulated the year-through dynamic operation at different level of hydrogen mobility penetration, considering the realistic loads in a typical residential district in the UK. In this section we present the results of our study. Section 4.1 provides the operating map of the rSOC stack resulting from the steady-state thermal-electrochemical model. This map is used for the time-resolved dynamic modeling of the system, whose main outcome is the definition of SOFC/SOEC schedules for each of the 24 typical days (Section 4.2) according to the daily self-sufficiency constraints explained in Section 3.4.1. Adopting the benchmark schedules identified in Section 4.2, in Section 4.3 we will list and discuss a set of performance indicators of the rSOC-based polygeneration system, the wind farm and the beneficial effect of the rSOC system as interface between the wind farm and the electric grid. The values of the performance indicators described in Section 3.5 (daily electric efficiency, daily global efficiency, annual efficiency and variation of the CO_2 emission with respect to a reference energy system) are thoroughly commented in Sections 4.4 and 4.5. It is worth clarifying that it is hard to compare the results of our analysis with those of other studies due to different system architectures and operating strategies (e.g., Baldinelli et al. [45] included a flywheel as a fast-responding storage unit additional to the rSOC stack, which stored excess PV production), location and size of the plant, energy source and backup options, modeling assumptions (e.g., rSOC operation in nominal condition in the work by Sorrentino et al. [18]), commodities produced by the plant (e.g., seawater desalination in [20]) and objective of the model (e.g., constrained optimization as in [19] versus the dynamic simulation in this study). However, all the results confirm the rSOC technology as a possible interface between energy demand and supply, playing a key role in the limitation of disturbances and fluctuation on/from the grid in a more resilient and integrated energy system.

4.1. Steady-state operating map of the rSOC system

The result of the steady-state simulations for SOFC/SOEC modes is an operating map describing the performance of the plant and the mutual exchange of mass and energy flows between the rSOC system and the external environment (i.e., hydrogen and thermal storages, DH scheme, wind farm, electricity grid and microgrid loads). This map (Table 3) is the key input for the simulation of the dynamic operation of the complete system (Section 3.4.1).

W_{BoP} is the total power input/output of the balance of plant (BoP) of the SOC stack. It is mainly related to the pressure conditioning of H_2, which is compressed in SOEC mode to reach the storage pressure, while it expands in turbine in SOFC mode from storage to stack pressure generating a power flow even exceeding that required from other auxiliaries (i.e., $W_{BoP} > 0$). The thermal balance of the BoP – Q_{BoP} – is negative in SOEC, mainly due to the heat requirement for steam generation, while it is positive in SOFC thanks to the lower preheating requirement and the heat recovery from water condensation.

The results show that steady-state CHP efficiency in SOFC is almost independent from the output power, while the SOEC one increases with the electrolyzer power. This is due to the increasing weight of thermal output: irreversibilities progressively balance the reaction endothermicity and allow the exothermic operation of the SOEC over the thermoneutral point. Considering only electricity generation (or hydrogen production, respectively) as the useful effect of the SOFC (or SOEC) operation, the electric efficiencies of the stack are computed: the difference between η_{EL} and η_{CHP} shows the weight of the heat fluxes leaving/entering the stack.

It is worth noting that the steady-state electric (Power-to-H_2-to-Power) roundtrip efficiency would be the product of the electric efficiencies of two operating points in SOFC and SOEC mode characterized by the same P_{H2} (i.e. provided that produced hydrogen is equal to the consumed hydrogen).

Table 3 - Results of the steady-state simulations of the rSOC plant

$W_{stack,AC}$	W_{BoP}	Q_{stack}	Q_{BoP}	P_{H2}	η_{EL}	η_{CHP}
MW_e	kW_e	MW_{th}	MW_{th}	MW	%	%
SOFC subsystem						
2	46	0.82	0.66	3.88	51.55	78.42
4	95	1.86	1.37	8.04	49.75	78.37
6	148	3.18	2.15	12.6	47.62	78.35
8	207	4.88	3.01	17.6	45.45	78.35
10	274	7.13	3.98	23.3	42.92	78.36
SOEC subsystem						
10	-590	-1.69	-0.57	8.45	84.50	75.11
20	-1080	-1.68	-1.05	15.6	78.00	77.05
30	-1510	-0.60	-1.47	21.8	72.67	78.54
40	-1912	1.24	-1.85	27.5	68.75	79.74
50	-2269	3.67	-2.19	32.7	65.40	80.72

Results of the pinch analysis for the system heat integration show (further details can be found in the supplementary material):

- in SOFC nominal conditions (i.e., 10 MW_{AC}), the availability of 3.7 MW from hot exhaust gases between 249 °C and 101.5 °C, useful for DH application, which is designed with 120/90 °C supply/return temperatures (Fig. A.3);
- in SOEC nominal conditions (i.e., 50 MW_{AC}), the need for 1.0 MW to complete the production and preheating of steam entering the cell stack from 542.7 °C to 700 °C. It is possible to extract this lacking heat from the high-temperature storage unit (HSU) operating at a temperature of 800 °C (Fig. A.4).

4.2. Benchmark SOFC- and SOEC-driven schedules

Once that the SOFC/SOEC schedules of the plant are computed for each of the 24 typical days – each week- and weekend day of the 12 months – according to the dynamic model described in Section 3.4, the model verifies the applicable constraints and discards the unfeasible schedules:

- the schedules with the lowest numbers of SOEC operating hours that do not meet H_2 self-sufficiency constraint because the stack is not able to produce the required hydrogen even at full SOEC power;
- the schedules with the lowest numbers of SOFC operating hours that do not meet thermal self-sufficiency constraint because they do not ensure enough heat to the HSU to sustain the larger number of SOEC hours in under-thermoneutral conditions.

The schedules that fulfill both the H_2 and thermal self-sufficiency constraints are valid. To assess the performance of the system, two benchmark schedules are considered among the valid ones per each typical day (Figure 3):

- *SOFC-driven* profile: it is the feasible schedule that presents the highest number of hours of SOFC operation. The hours of operation as electrolyzer are consequently minimized, leading the stack to operate at high SOEC power, close or even over the thermoneutral point (i.e., at high power density). With this profile, electricity (and heat, consequently) production is maximized.
- *SOEC-driven* profile: it is the feasible schedule with the largest number of SOEC hours. This profile limits the SOFC operation in the hours of the day with the highest electric price, with the minimum fraction of microgrid electricity demand covered by the rSOC plant. In this operating schedule, the capacity factor of the electrolyzer is the minimum, because the total hydrogen demand is the lowest – due to the lowest number of SOFC hours – and its production is distributed on the largest number of hours: thus, the SOEC works at very low partial loads.

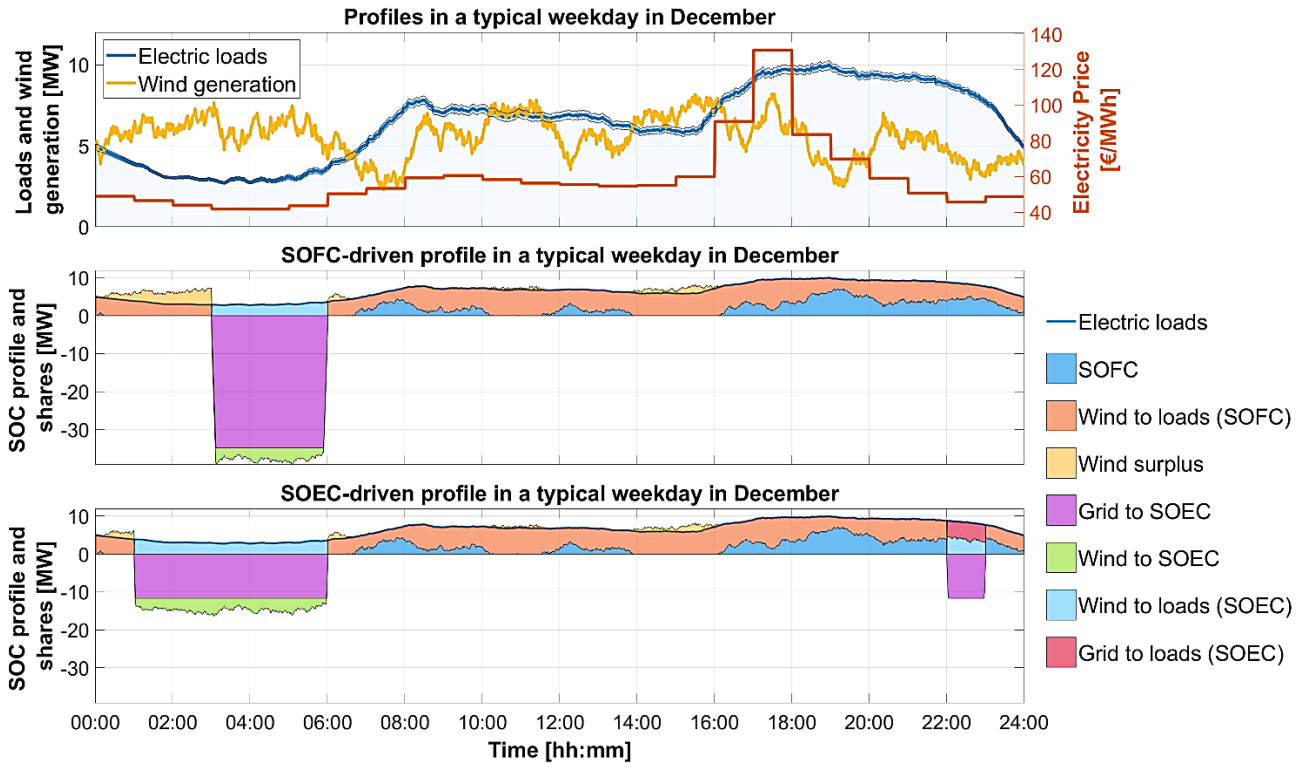

Figure 3 - Outcome of the electric module of the simulation for a weekday in December in case of reference H_2 mobility demand

Figure 3 (top) highlights the mismatch between power demand (blue line, shown also in the center and bottom figures) and wind power production (yellow line) on a typical weekday in December. Considering the hourly profile of electricity price (red line in top figure), the fuel cell operation in *SOEC-driven* schedule (bottom figure) lasts 18 hours. The SOFC production (blue areas) integrates the energy produced by the wind farm and supplied to the district (orange areas). In limited time lapses, the wind power production exceeds the demand and is provided to the distribution grid (yellow areas), while the SOFC is set in hot stand-by. During SOEC operation, wind energy is the primary source that fulfills the loads (light-blue areas). If wind power surplus is not sufficient to feed electrolysis (green areas), electricity is imported from the grid to satisfy the H_2 self-sufficiency constraint (purple areas). If wind power production is less than the district demand, part of the loads is fulfilled by grid electricity (red areas). *SOFC-driven* schedule in Figure 3 (center) highlights the higher power rate during SOEC operation to meet the H_2 self-sufficiency constraint in the shrunk time slots for electrolysis.

All the other allowed schedules lead to intermediate results between *SOEC-* and *SOFC-driven* profiles, thus were not considered in the analysis.

4.3. System performance

The performance of the polygeneration system was evaluated for one year of operation considering the variation of polygeneration mix. Table 4 shows: the district electricity demand covered by the rSOC system ($E_{SOFC,load,y}$), the number of operating hours in SOFC ($h_{SOFC,y}$), the DH heat provided by the HSU ($E_{DH,y}$) and the corresponding number of houses served (N_h) and the capacity factors ($CF_{SOEC/SOFC}$). The capacity factor of SOFC (or SOEC, respectively) is computed as the ratio of the yearly energy produced (or consumed) to the product of nominal size of SOFC (or SOEC) times the operating hours as SOFC (or SOEC). While the SOEC capacity factor is determined by the hydrogen demand, the SOFC capacity factor is determined by the match of electric demand and the wind power output profile, as the plant is working in load-following to supply the fraction of the load not covered by wind power.

Concerning the *SOFC-driven* operating profile (left side of Table 4), the increase of hydrogen demand for mobility reduces the amount of hydrogen available for re-electrification and, due to the hydrogen self-sufficiency constraint, the number of SOFC operating hours also decreases. As a consequence, also the electricity provided by the SOFC to the microgrid loads decreases, from the 34.5% to the 32.6% of the total district demand. The CF_{SOFC} has the opposite trend: it increases because the remaining SOFC hours are those in which the load demand is higher and thus the SOFC works averagely at higher power level, closer to the nominal one. Also the CF_{SOEC} has the same trend, as the SOEC works progressively at higher power due to the increasing hydrogen demand. From the thermal point of view, the reduction of the number of operating hours in SOFC is partially compensated by the higher power – and thus thermal losses – of the stack. On the other hand, the *SOFC-driven* schedule leads the SOEC to work at the nominal condition (over thermoneutral point), as shown by the high capacity factor of SOEC in Table 4: this trend mitigates the mentioned reduction of thermal availability from SOFC exothermic operation, leading to a slightly increasing thermal energy output to the DH, visible for a H_2 penetration higher than 5.

In the *SOEC-driven* profile (right side of Table 4), the limited duration of SOFC operation determines a lower share of electricity demand covered by the rSOC system ($E_{SOFC,load,y}$) if compared to the *SOFC-driven* profile, for all the levels of hydrogen penetration. Electrolysis occurs in the endothermic region of the polarization curve, as shown by the low CF_{SOEC}, due to the higher number of SOEC operation hours that determine the stack operation at lower power levels. However, the increasing generation of mobility hydrogen determines a progressive shift of the absorbed electric power in SOEC mode to the value corresponding to the peak thermal demand of the stack. Therefore, the SOFC hours increase to ensure the plant thermal self-sufficiency. This trend reverses for a H_2 penetration higher than 5, as SOEC starts to work over the point of peak endothermic flux: the weight of H_2 re-electrification in SOFC mode reduces and the thermal supply to DH increases.

Table 4 - System performance with variation of the polygeneration mix

H_2 mobility penetration (demand in ton/y)	***SOFC-driven* operating profile**			***SOEC-driven* operating profile**		
	$E_{SOFC,load,y}$ (GWh, $\%E_{load,y}$)	$E_{DH,y}$ (GWh)	CF_{SOFC} (%)	$E_{SOFC,load,y}$ (GWh, $\%E_{load,y}$)	$E_{DH,y}$ (GWh)	CF_{SOFC} (%)
	$h_{SOFC,y}$ (h/year)	N_h (-)	CF_{SOEC} (%)	$h_{SOFC,y}$ (h/year)	N_h (-)	CF_{SOEC} (%)
0.1	17.9 (34.5%)	9.06	28.99%	13.5 (26.1%)	0.175	30.02%
(9.77)	6,162	2,000	29.69%	4,474	40	11.77%
0.2	17.9 (34.5%)	9.06	29.07%	13.7 (26.5%)	0.203	29.91%
(19.53)	6,139	2,000	29.71%	4,571	50	12.49%
0.5	17.9 (34.5%)	9.06	29.07%	14.4 (27.7%)	0.357	29.83%
(48.82)	6,139	2,000	30.80%	4,796	80	14.53%
1	17.8 (34.5%)	9.06	29.08%	14.9 (28.7%)	0.421	29.81%
(97.65)	6,136	2,000	32.61%	4,973	100	16.98%
2	17.8 (34.4%)	9.06	29.20%	15.4 (29.7%)	0.653	29.86%
(195.3)	6,098	2,000	35.69%	5,133	150	20.90%
5	17.6 (33.9%)	9.52	29.34%	15.6 (30.1%)	0.948	29.93%
(488.2)	5,986	2,100	44.54%	5,197	210	29.41%
10	16.9 (32.6%)	9.52	29.41%	15.0 (29.1%)	1.03	29.89%
(976.5)	5,727	2,100	55.07%	5,018	230	40.20%

Of the total annual production of the wind power plant (37.2 GWh), most is directly supplied to the loads (33.8 GWh, see Figure 4), a smaller fraction to the SOEC (from 1.27 to 2.74 GWh, corresponding to 3-11% of the total annual electric input for electrolysis, $E_{SOEC,y}$) and the remaining part to the grid (from 0.71 to 2.17 GWh), as shown in Table 5. It is worth noting that the share of wind energy supplied to the grid in the *SOFC-driven* strategy is from 3% to 6%, while it is lower than 3% in the *SOEC-driven* one due to the lower SOFC availability (i.e., more wind energy absorbed by the microgrid). Hence, in energy terms the wind-farm contribution to the grid is almost negligible.

Table 5 - Utilization of wind power production

H_2 mobility penetration (demand in ton/y)	***SOFC-driven* profile**				***SOEC-driven* profile**			
	$E_{wind,SOEC,y}$ (GWh, $\%E_{SOEC,y}$)	$E_{wind,grid,y}$ (GWh, $\%E_{wind,y}$)	$\hat{P}_{wind,grid,y}$ (MW)	$h_{wind,grid,y}$ (h/year)	$E_{wind,SOEC,y}$ (GWh, $\%E_{SOEC,y}$)	$E_{wind,grid,y}$ (GWh, $\%E_{wind,y}$)	$\hat{P}_{wind,grid,y}$ (MW)	$h_{wind,grid,y}$ (h/year)
0.1 (9.77)	1.27 (3.30%)	2.17 (5.84%)	4.483	1,557	2.74 (10.8%)	0.71 (1.91%)	4.035	703
0.2 (19.53)	1.33 (3.43%)	2.11 (5.68%)	4.483	1,533	2.74 (10.5%)	0.71 (1.91%)	4.035	705
0.5 (48.82)	1.36 (3.36%)	2.09 (5.62%)	4.483	1,511	2.59 (8.98%)	0.86 (2.31%)	4.035	782
1 (97.65)	1.47 (3.45%)	1.97 (5.30%)	4.483	1,437	2.55 (7.93%)	0.90 (2.41%)	4.035	807
2 (195.3)	1.52 (3.20%)	1.93 (5.17%)	4.483	1,404	2.48 (6.53%)	0.97 (2.61%)	4.035	854
5 (488.2)	1.88 (3.04%)	1.57 (4.22%)	4.483	1,233	2.44 (4.66%)	1.01 (2.71%)	4.035	872
10 (976.5)	2.32 (2.77%)	1.13 (3.04%)	4.035	977	2.58 (3.43%)	0.87 (2.33%)	4.035	803

In terms of power, the maximum power input to the grid from the wind farm (yellow areas in Figure 3) is 4.5 MW, which occurs during SOFC operation at night on the weekend days in February. This represents a significant reduction of the peak input, as the wind farm alone would have provided a maximum peak of 15 MW to the grid. It is worth noting that the direct supply of electricity from the wind farm to the grid occurs only for 1,000-1,600 hours during the year ($h_{wind,grid,y}$) in *SOFC-driven* operation, with an average power input of about 1.3 MW. The shrinkage of SOFC operation in *SOEC-driven* strategy reduces the availability of surplus wind electricity directly supplied to the grid, as suggested by the reduced values of $h_{wind,grid,y}$ (700-870 hours/year). Hence, a larger share of $E_{wind,y}$ can be used to feed water electrolysis ($E_{wind,SOEC,y}$) in *SOEC-driven* strategy thanks to the higher probability of having excess wind power production in the hours of SOEC operation (green areas in Figure 3).

The wind power production exceeding the microgrid electric loads is too low to fulfill completely the electricity input for water electrolysis during SOEC operation: this share is about 3% if *SOFC-driven* schedule is adopted, while it reduces from 10.8% to 3.43% with the increasing hydrogen mobility penetration in *SOEC-driven* strategy (Table 5). Hence, from 89% to 97% of the SOEC input electricity is actually provided by the grid (purple areas in Figure 3). However, with the adopted logic (Section 3.3.1), the grid electricity compensating the frequent wind power shortages during SOEC operation has a flat power rate (purple areas in Figure 3), hence reducing the impact of wind intermittence on the distribution grid.

The electric energy produced by the dedicated wind farm limits the peak demand of the residential district satisfied directly by the grid during SOEC operation (red areas in Figure 3). With the *SOEC-driven* strategy – and also *SOFC-driven* strategy, but only with H_2 penetration equal to 10 – the peak power provided from the grid to the district microgrid is 6.46 MW (about 35% less than the annual peak of 10 MW) and corresponds to the maximum mismatch between electric demand and wind power output, which is occurring at night on weekdays in October (red areas in Figure B.1 of supplementary materials). Concerning the *SOFC-driven* strategy with H_2 penetration between 0.1 and 5, the peak demand not directly fulfilled by wind power generation is 3.9 MW (early morning on weekend days in June, see red areas in Figure B.2 of supplementary materials). Hence, although the loads are not completely disconnected from the grid during SOEC operation, the adopted logic limits the disturbances on the grid in terms of both peak demand of the district and fluctuations of the installed RES plant.

With the *SOFC-driven* operating profile, a larger fraction of the yearly electricity demand of the microgrid ($E_{load,y}$) not directly fulfilled by the wind farm is covered by the SOFC, from 34.5% to 32.6% with the increasing hydrogen demand for mobility (orange bars in Figure 4). The use of grid electricity to feed the microgrid is very limited, from 0.3% to 2.2% of $E_{load,y}$.

From the point of view of thermal loads, the *SOFC-driven* schedule allows to provide heating to a larger number of households (around 2,000). This could balance the lower efficiency of this schedule (see Section 4.4 for discussion) and also the higher indirect emissions (see Section 4.5) connected to the use of not fully renewable grid-electricity, especially to feed water electrolysis (from 96.7% to 97.23% of the SOEC electricity input with the increasing hydrogen demand for mobility). In general, this type of schedule could be suitable for an application in which the users (i.e., the local microgrid) must be disconnected from the grid for a large number of hours, have a high heating demand and the grid electricity has a low carbon intensity.

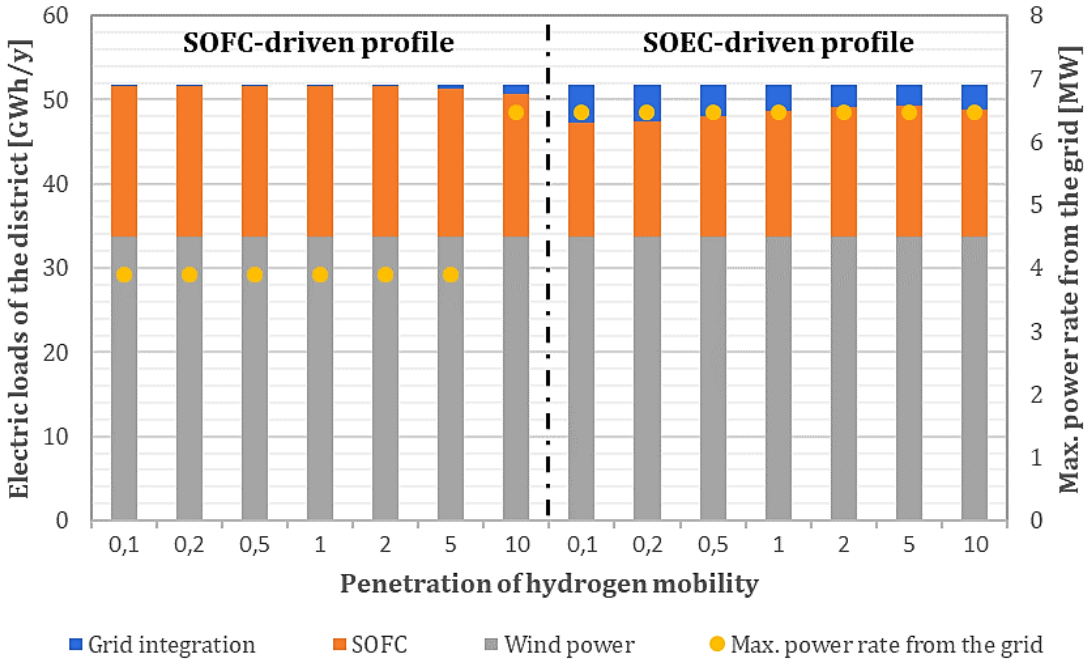

Figure 4 - Coverage of the residential electric loads and maximum electric input from the grid throughout the year

The *SOEC-driven* operating profile is the one more oriented towards hydrogen production, with SOFC covering 26.1%-29.1% of the electricity demand (Figure 4). This type of schedule is suitable for a plant installed in a district with a reliable grid connection and a contained heat demand (e.g., hot climate location), providing grid services to the district in a limited number of hours.

Hence, what actually changes for both the schedule types with the variation of the hydrogen mobility demand is the number of hours of operation in fuel cell mode (while still imposing the self-sufficiency constraints presented in Section 3.4.1) and the residual thermal availability that can feed the DH scheme ($E_{DH,y}$) in order to close the annual energy balance on the HSU.

4.4. Efficiency

Figure 5 shows the trends of the daily electric efficiency $\eta_{d,p}$ and daily global efficiency $\eta^*_{d,p}$ for different operational profiles in every typical day, considering the reference H_2 mobility demand (penetration equal to 1). The efficiency is depicted in bands: lower and upper bounds represent the daily electric efficiency (Eq. 6) and the daily global efficiency (Eq. 7), respectively.

The assumption of a linear polarization with fixed steam/hydrogen utilization entails that the cells operate more efficiently at low currents and thus at low capacity factors: the lower voltage in SOEC mode near OCV implies a lower power consumed per unit of produced hydrogen and vice versa for the SOFC mode, with higher power produced per unit of hydrogen at low current. For this reason, the strategy that ensures a larger number of operating hours at lower CF can guarantee a higher efficiency. Therefore, considering the capacity factors associated to the reference H_2-mobility demand, the *SOEC-driven* mode ensures the higher efficiency, especially during the summer period when the H_2 mobility demand is smaller (thus the stack efficiency for hydrogen generation is higher). It is worth noting that operating at low current in SOEC means to work in an endothermic regime, but the thermal self-sufficiency ensured by the HSU prevents the efficiency penalty due to providing external heat.

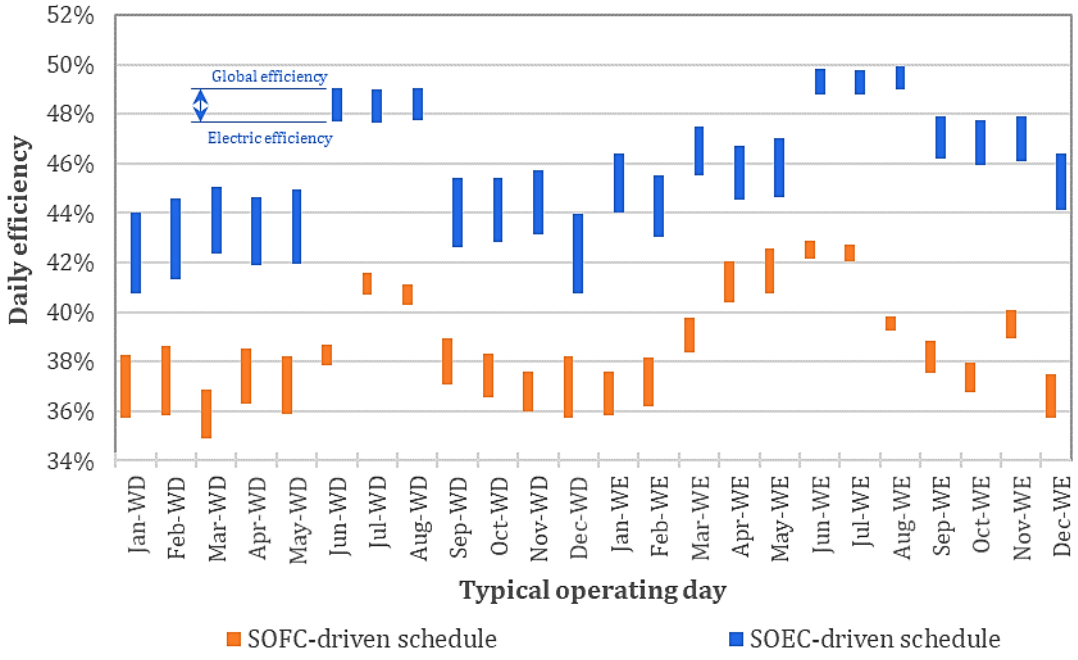

Figure 5 - Trend of the daily efficiency (electric and global) throughout the year with the reference demand of H_2 for mobility

Figure 5 also highlights the limited weight of the energy output associated to mobility hydrogen with respect to the Power-to-Power scheme, especially in the case of *SOFC-driven* schedule, as the difference between the global and electric efficiency is limited to few %. However, the *SOFC-driven* scheme is the one that ensures a larger amount of heat available in the HSU for the DH application, even if less efficient from the point of view of produced electricity and mobility hydrogen. This is visible from the results reported in Table 4: the rSOC system controlled with the *SOEC-driven* strategy provides heating by DH to a sensibly lower number of houses than with the *SOFC-driven* one, for all the values of mobility penetration.

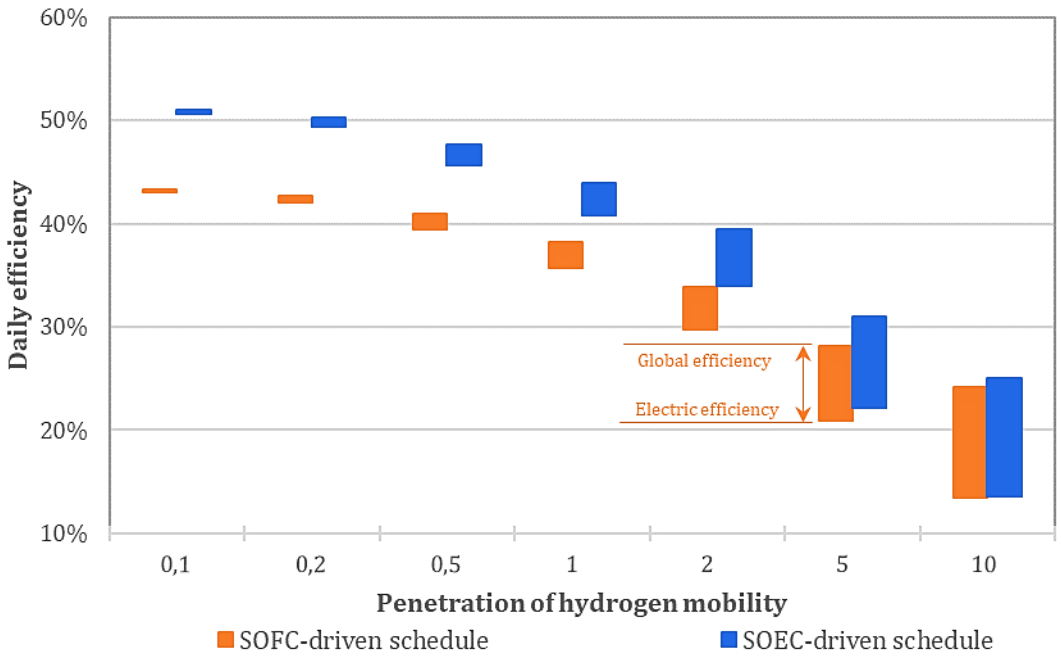

Figure 6 - Variation of efficiency (electric and global) with H_2 demand (referred to weekdays in December)

Figure 6 highlights how the daily efficiency is affected by the penetration of H_2 demand (the reference weekday of December is used) showing a remarkable gap between $\eta_{d,p}$ and $\eta^*_{d,p}$ only for hydrogen mobility penetration higher than 1: they both feature a monotonic decreasing trend (due to increasing CF_{SOEC}). However, $\eta^*_{d,p}$ stands beyond 20% even against the highest demand for H_2 mobility.

Figure 7 shows that the annual efficiency of the *SOFC-driven* scheme reaches a maximum of 71% with the minimum demand of mobility H_2 and keeps being the highest at even larger values of hydrogen penetration. This is due to the large amount of heat available in the HSU for the DH when the SOFC operation is favored. The *SOEC-driven* strategy shows an annual efficiency that increases with the hydrogen penetration – from 55% to 61% – because of the shifting of the SOEC operation towards the nominal point (i.e., higher CF), consequently moving to an exothermic regime. This result demonstrates that the heat commodity plays a major role for the efficient operation of the rSOC plant. Moreover, a larger H_2 demand (penetration much higher than 10) could be managed with a *SOEC-driven* control strategy in a more efficient way thanks to the higher amount of heat available for the DH.

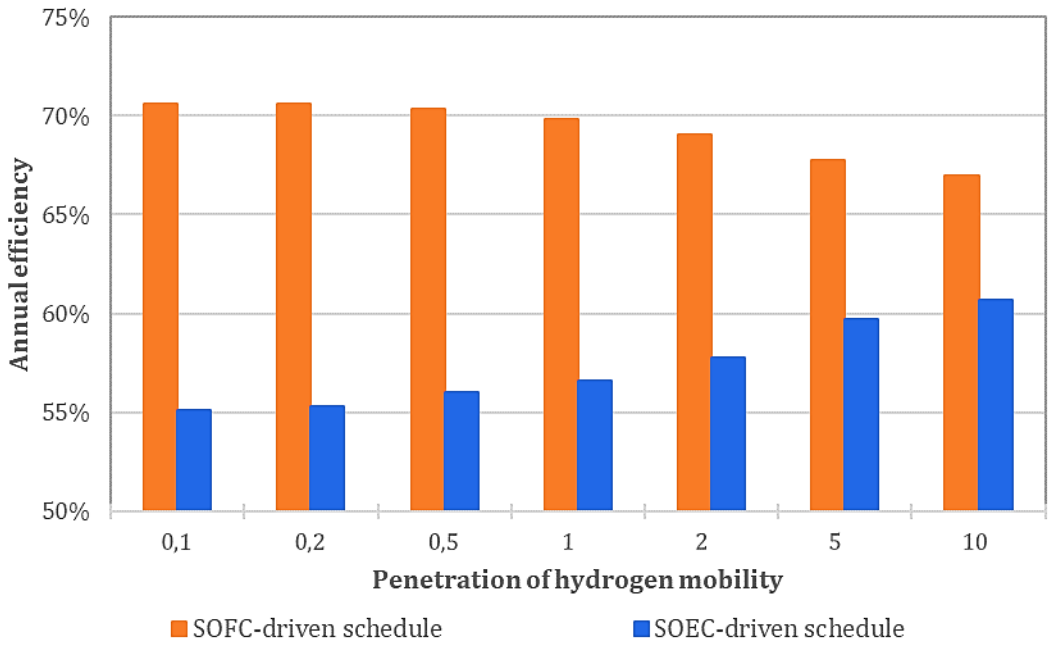

Figure 7 - Variation of the annual efficiency with the H_2 demand

4.5. Evaluation of CO_2 emissions

As shown before, the share of electricity and DH demand covered by the rSOC plant depends not only on the penetration of H_2 mobility, but also on the adopted control scheme. For this reason, the CO_2 emissions of the reference energy system (Section 3.5.3) that meets the same demand of the rSOC plant (following either the *SOFC-* or the *SOEC-driven* schedule) vary as shown in Figure 8 (top).

Figure 8 (bottom) depicts the indirect CO_2 emissions related to the operation of the rSOC system due to the use of grid electricity, which is necessary in case of wind power shortage. Two contributions can be identified: i) the grid electric energy consumed by SOEC to drive electrolysis, and ii) the electric energy directly supplied by the grid to the residential loads in case of insufficient wind power generation when rSOC is working as SOEC. The *SOEC-driven* profile shows smaller CO_2 emissions to drive electrolysis because a lower amount of H_2 is produced for re-electrification (i.e., less electricity is consumed by the SOEC). On the other hand, a larger share of the electric demand (5.7-8.7%, decreasing with the increasing hydrogen demand for mobility) is fulfilled directly by the grid (Figure 4) with this schedule: notice that blue bars in Figure 8 (bottom) are higher than those of the *SOFC-driven* profile. However, as the direct use of electricity from the grid to fulfil the microgrid demand prevents the energy losses related to power-to-H_2-to-power roundtrip conversion, the contribution of this last item is minor. Hence, the global emissions of CO_2 are lower when rSOC adopts *SOEC-driven* operating profile.

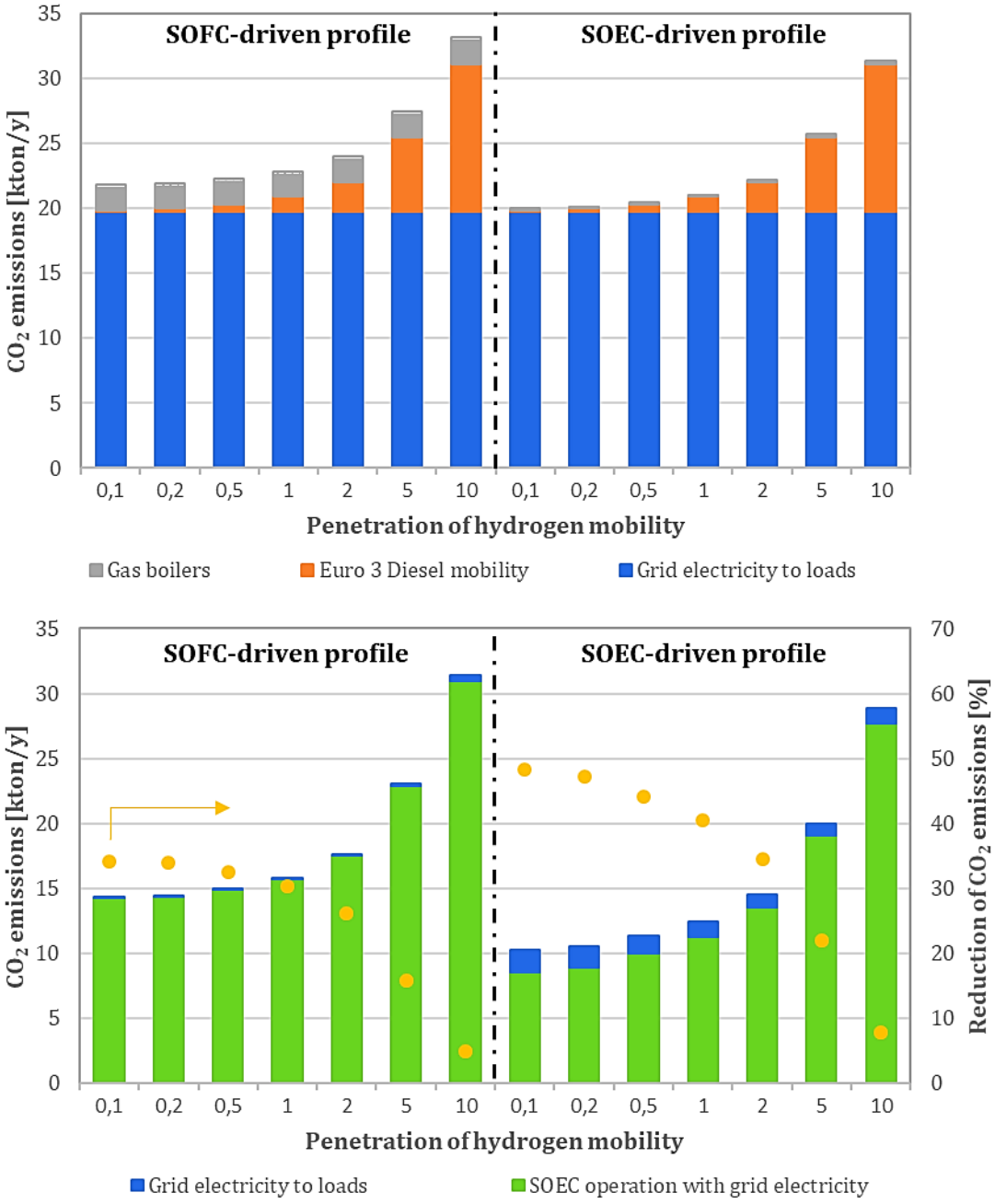

Figure 8 – Carbon dioxide emissions of the reference energy system (top) and of the rSOC plant (bottom, with % decrease)

Figure 8 (bottom) also depicts the CO_2 emissions decrease (dots), which is calculated as difference with the reference scenario. The rSOC system allows to eliminate the emissions related to Diesel-fueled buses and gas-fired boilers and part of the emissions associated to the grid electricity used to fulfill the loads of the residential district. The emissions savings decrease for both types of operating schedule with the increasing H_2 demand. This is due to the increasing electricity consumption from the SOEC, which is mostly covered by grid electricity with

the assumed size of the wind plant. If a larger wind power farm was installed, the amount of renewable electricity feeding the SOEC would increase, allowing higher emissions savings also when the H_2 demand level is larger. However, a higher wind power would imply more fluctuations for the grid. This is an unavoidable drawback: more renewable power increases the possible CO_2 savings at the cost of larger power fluctuations, unless a stable renewable source or a larger power-to-H_2-to-power system is adopted.

It is worth highlighting that an rSOC system fed only by the grid (i.e., without a dedicated RES plant) would result in no environmental advantages with respect to the reference energy system: the carbon intensity of grid electricity is 381.46 g/kWh and the rSOC system will always require more energy than a directly connected user since the overall efficiency is less than one. On the other hand, the mission of the rSOC system gains consideration only in the presence of a locally available intermittent RES plant: the SOEC/SOFC operation can be scheduled day-by-day to store zero-emission renewable energy in the form of hydrogen and then diversify it in different market commodities (i.e., hydrogen, re-electrification, heat) following the Power-to-X protocol. Moreover, the proposed polygeneration system has the advantage of withdrawing the distributed sources of CO_2 emissions (i.e., buses and gas boilers) in stationary centralized energy production plants that could be retrofitted with advanced techniques for carbon capture and emission control.

The variation of the CO_2 emissions with respect to a reference scenario including only a grid-connected wind power farm (i.e., without an rSOC buffering system) is also interesting. Referring to Figure 8 (top), blue bars (19.75 ton_{CO2}/y) derive from fulfilling the annual electric demand of 51.76 GWh with grid electricity; instead, the introduction of electric RES would not affect the emissions of gas boilers (grey bars) and Diesel buses (orange bars). Since the wind farm can provide 33.8 GWh/y to the microgrid, the emissions associated to the district electric consumption would decrease to 6.85 ton_{CO2}/y. Hence, the logic chosen for the SOFC/SOEC switching in our case study (Section 3.4.1) would not be the best from the environmental point of view (due to the extensive use of grid electricity to drive electrolysis in off-peak hours, as shown by green bars in Figure 8 – bottom). However, this is an incomplete and unfair comparison because the RES-only scenario would not account for the Power-to-X conversion and the grid services provided by the rSOC system. In particular, the estimation of other performance parameters (e.g., wind power curtailment, reduction of peak demand on the grid) and scenarios would confirm the importance of an interface (the rSOC system in our case study or other storage and power-shifting devices [3]) between power demand and intermittent supply. For the sake of conciseness, these interesting issues were not fully dealt with in this paper and will be taken into account in future works.

From the economic point of view, the flexibility of the rSOC system would allow to follow the intra-day electricity market and maximize the operating profitability, while the compactness of the rSOC system allows to reduce the initial capital expenditure. In the future, a higher share of curtailment will presumably be available to feed electrolysis and the compression of hydrogen for both storage (30 bar) and refueling. This will make the

polygeneration system attractive for the synergic management of both RES surplus and demand of energy in different forms and even more environmentally competitive.

5. Conclusions

Based on the dynamic analysis performed, this study supports the use of hydrogen as a sustainable energy carrier, aiming to harmonize the diffusion of renewable sources in the energy generation portfolio. The study assesses the energy and environmental performance of a 10/50 MW (fuel cell/electrolysis) rSOC plant fed preferentially with a 15-MW dedicated wind farm. Following a flexible Power-to-X schedule, the system can store electricity in the form of hydrogen for time-shifted electric power delivery and decarbonize different final energy uses by providing hydrogen for mobility and heat for the local district heating network through a high-temperature molten-NaCl storage. Thanks to the interposition of a hydrogen storage, the proposed polygeneration plant can also mitigate the impact of the fluctuations of local RES generation on the electric grid by disconnecting local loads during the peak-demand hours. The Power-to-X solution proposed aims to increase the reliability of power supply by dynamically interconnecting the electric grid to other infrastructures (e.g., district heating scheme, hydrogen mobility, wind farm) and to further the multi-sectorial decarbonization of economy.

A method is introduced for the component-to-system modeling and the dynamic analysis of a grid-connected Power-to-X system and a logic is proposed for the smart management of the different storage units. Different utilization strategies and SOFC/SOEC scheduling options were analyzed and compared in terms of technical and environmental performances under self-sufficiency constraints for both heat and hydrogen vectors aiming to reduce the plant size and rationalize the Power-to-X conversion and storage. We performed a comprehensive feasibility study of the proposed system at different levels of hydrogen-fed mobility penetration and simulated its year-through operation in a district-sized urban context. The main findings of this work are summarized below:

- Heat commodity plays a major role for the efficient operation of an rSOC polygeneration plant. The polygeneration system results in an annual efficiency that ranges from 55 to 70% (including also thermal energy delivered to DH scheme), according to the adopted operating profile and the hydrogen mobility penetration.
- The rSOC system is able to effectively integrate the wind production on the microgrid and to significantly smooth the power fluctuations on the electricity distribution grid. While the wind farm can supply up to 65% of the microgrid electricity demand, the rSOC is able to provide as much as 26% to 35%, with only a small fraction (< 10%) required from the grid. The power peak required by the microgrid to the grid is reduced by 35% and the input power peak from the wind farm to the grid is reduced by 70%.

- The adoption of an *SOFC-driven* operating profile ensures the thermal availability for a DH scheme serving about 2,000 houses; the number of served houses goes down to 40-230 in case of *SOEC-driven* profile.
- A 5-50% decrease of CO_2 emissions with respect to a reference energy system (in which electric, thermal and mobility demands are covered by grid electricity, gas boilers and diesel buses, respectively) if the rSOC plant is fed preferentially by a dedicated wind farm and by electricity with the current UK emission factor in case of wind power shortages.
- A sensitivity analysis detected the detrimental effect of the increasing penetration of SOEC-fed H_2 mobility on the daily electric efficiency of the rSOC system, with a reduction from 45-50% in the reference case to 15% in an ambitious scenario foreseeing a widespread diffusion of low-impact vehicles. The same trend is found for the daily global efficiency, which takes into account also hydrogen as a useful output.
- From an environmental point of view, the increase of H_2 mobility demand reduces the emissions savings. Hence, with the proposed sizes and operating strategy, the rSOC plant has a better energy and environmental performance in supporting renewable electricity integration on the microgrid, rather than providing mobility hydrogen.

As a general result that can be useful for the evaluation of real applications of the rSOC concept, the analysis of the different operating strategies showed that the *SOEC-driven* schedule, which is more oriented towards hydrogen production, is suitable for plants installed in districts with a reliable grid connection and a limited heat demand, while the *SOFC-driven* schedule fits best the micro-grids with limited grid connection and high heating demand, and where the grid electricity has a low carbon intensity.

The present work paves the way for a series of future works aiming to define in detail and optimize the layout and the operating strategy of the system. An important issue that has not been taken into account in the analysis is the economic feasibility of the plant: a focus on the monetary cash flows and economic profitability associated to the installation and operation of the plant would investigate the attractiveness of the rSOC plant as an early Power-to-X polygeneration system. Modeling efforts are also necessary to reliably simulate the dynamic behavior of the rSOC system including its degradation, in either grid-connected or remote off-grid configuration.

FUNDING

This research did not receive any specific grant from funding agencies in the public, commercial, or not-for-profit sectors.

REFERENCES

[1] United Nations, “The Sustainable Development Goals Report,” New York, 2018.

[2] P. D. Lund, J. Lindgren, J. Mikkola, and J. Salpakari, “Review of energy system flexibility measures to enable high levels of variable renewable electricity,” *Renew. Sustain. Energy Rev.*, vol. 45, pp. 785–807, May 2015.

[3] G. Buffo, P. Marocco, D. Ferrero, A. Lanzini, and M. Santarelli, “Power-to-X and Power-to-Power routes,” in *Solar Hydrogen Production: Processes, Systems and Technologies*, Elsevier, 2019, pp. 530–575.

[4] B. Nastasi and G. Lo Basso, “Hydrogen to link heat and electricity in the transition towards future Smart Energy Systems,” *Energy*, vol. 110, pp. 5–22, Sep. 2016.

[5] C. J. Quarton and S. Samsatli, “Power-to-gas for injection into the gas grid: What can we learn from real-life projects, economic assessments and systems modelling?,” *Renew. Sustain. Energy Rev.*, vol. 98, pp. 302–316, 2018.

[6] S. Y. Gómez and D. Hotza, “Current developments in reversible solid oxide fuel cells,” *Renew. Sustain. Energy Rev.*, vol. 61, pp. 155–174, 2016.

[7] H. Æ. Sigurjonsson and L. R. Clausen, “Solution for the future smart energy system: A polygeneration plant based on reversible solid oxide cells and biomass gasification producing either electrofuel or power,” *Appl. Energy*, vol. 216, no. August 2017, pp. 323–337, 2018.

[8] M. Rokni, “Analysis of a polygeneration plant based on solar energy, dual mode solid oxide cells and desalination,” *Int. J. Hydrogen Energy*, vol. 44, no. 35, pp. 19224–19243, 2019.

[9] V. Venkataraman *et al.*, “Reversible solid oxide systems for energy and chemical applications – Review & perspectives,” *J. Energy Storage*, vol. 24, no. May, p. 100782, 2019.

[10] Y. Luo, Y. Shi, Y. Zheng, and N. Cai, “Reversible solid oxide fuel cell for natural gas/renewable hybrid power generation systems,” *J. Power Sources*, vol. 340, pp. 60–70, Feb. 2017.

[11] G. Vialetto, M. Noro, P. Colbertaldo, and M. Rokni, “Enhancement of energy generation efficiency in industrial facilities by SOFC – SOEC systems with additional hydrogen production,” *Int. J. Hydrogen Energy*, 2019.

[12] A. Baldinelli, L. Barelli, and G. Bidini, “Progress in renewable power exploitation: reversible solid oxide cells-flywheel hybrid storage systems to enhance flexibility in micro-grids management,” *J. Energy*

Storage, 2019.

[13] S. Santhanam, M. P. Heddrich, M. Riedel, and K. A. Friedrich, "Theoretical and experimental study of Reversible Solid Oxide Cell (r-SOC) systems for energy storage," *Energy*, vol. 141, pp. 202–214, Dec. 2017.

[14] C. H. Wendel and R. J. Braun, "Design and techno-economic analysis of high efficiency reversible solid oxide cell systems for distributed energy storage," *Appl. Energy*, vol. 172, pp. 118–131, 2016.

[15] N. Perdikaris, K. D. Panopoulos, P. Hofmann, S. Spyrakis, and E. Kakaras, "Design and exergetic analysis of a novel carbon free tri-generation system for hydrogen, power and heat production from natural gas, based on combined solid oxide fuel and electrolyser cells," *Int. J. Hydrogen Energy*, vol. 35, no. 6, pp. 2446–2456, 2010.

[16] P. Kazempoor and R. J. Braun, "Model validation and performance analysis of regenerative solid oxide cells for energy storage applications: Reversible operation," *Int. J. Hydrogen Energy*, vol. 39, no. 11, pp. 5955–5971, 2014.

[17] F. Lonis, V. Tola, and G. Cau, "Renewable methanol production and use through reversible solid oxide cells and recycled CO2 hydrogenation," *Fuel*, vol. 246, pp. 500–515, 2019.

[18] M. Sorrentino, A. Adamo, and G. Nappi, "Self-Sufficient and Islanded-Oriented Design of a Reversible Solid Oxide Cell-Based Renewable Microgrid," *Energies*, vol. 12, no. 3224, 2019.

[19] L. Tribioli, R. Cozzolino, L. Evangelisti, and G. Bella, "Energy management of an off-grid hybrid power plant with multiple energy storage systems," *Energies*, vol. 9, no. 8, 2016.

[20] N. C. Ullvius and M. Rokni, "A study on a polygeneration plant based on solar power and solid oxide cells," *Int. J. Hydrogen Energy*, vol. 44, no. 35, pp. 19206–19223, 2019.

[21] J. Mermelstein and O. Posdziech, "Development and Demonstration of a Novel Reversible SOFC System for Utility and Micro Grid Energy Storage," *Fuel Cells*, vol. 17, no. 4, pp. 562–570, 2017.

[22] D. Hickey, M. Cassidy, J. McElroy, F. Mitlitsky, and V. Venkataraman, "Optimization and Demonstration of a Solid Oxide Regenerative Fuel Cell System," in *ECS Proceedings Volumes*, 2005, vol. 2005–07, no. October 2003, pp. 285–294.

[23] P. Mottaghizadeh, S. Santhanam, M. P. Heddrich, K. A. Friedrich, and F. Rinaldi, "Process modeling of a reversible solid oxide cell (r-SOC) energy storage system utilizing commercially available SOC reactor," *Energy Convers. Manag.*, vol. 142, pp. 477–493, 2017.

[24] M. Dillig and J. Karl, "Thermal management of high temperature solid oxide electrolyser cell/fuel cell

systems," *Energy Procedia*, vol. 28, pp. 37–47, 2012.

[25] M. Dillig, J. Leimert, and J. Karl, "Planar high temperature heat pipes for SOFC/SOEC stack applications," *Fuel Cells*, vol. 14, no. 3, pp. 479–488, 2014.

[26] S. Santhanam, C. Schilt, B. Turker, T. Woudstra, and P. V. Aravind, "Thermodynamic modeling and evaluation of high efficiency heat pipe integrated biomass Gasifier–Solid Oxide Fuel Cells–Gas Turbine systems," *Energy*, vol. 109, pp. 751–764, Aug. 2016.

[27] P. Marocco, D. Ferrero, A. Lanzini, and M. Santarelli, "Benefits from heat pipe integration in H2 /H2O fed SOFC systems," *Appl. Energy*, vol. 241, pp. 472–482, 2019.

[28] K. Schwarze, O. Posdziech, S. Kroop, N. Lapeña-Rey, and J. Mermelstein, "Green industrial hydrogen via reversible high-temperature electrolysis," *ECS Trans.*, vol. 78, no. 1, pp. 2943–2952, 2017.

[29] M. Liu, W. Saman, and F. Bruno, "Review on storage materials and thermal performance enhancement techniques for high temperature phase change thermal storage systems," *Renew. Sustain. Energy Rev.*, vol. 16, no. 4, pp. 2118–2132, 2012.

[30] J. V. Paatero and P. D. Lund, "A model for generating household electricity load profiles," *Int. J. Energy Res.*, vol. 30, no. 5, pp. 273–290, 2006.

[31] J. Ortiz, F. Guarino, J. Salom, C. Corchero, and M. Cellura, "Stochastic model for electrical loads in Mediterranean residential buildings: Validation and applications," *Energy Build.*, vol. 80, pp. 23–36, 2014.

[32] I. Richardson, M. Thomson, D. Infield, and C. Clifford, "Domestic electricity use: A high-resolution energy demand model," *Energy Build.*, vol. 42, no. 10, pp. 1878–1887, 2010.

[33] I. Richardson, M. Thomson, D. Infield, and A. Delahunty, "Domestic lighting: A high-resolution energy demand model," *Energy Build.*, vol. 41, no. 7, pp. 781–789, 2009.

[34] T. Huld, R. Mueller, and A. Gambardella, "A new solar radiation database for estimating PV performance in Europe and Africa," *Sol. energy*, vol. 86, pp. 1803–1815, 2012.

[35] FCH-JU Fuel Cell and Hydrogen Joint Undertaking, "Multi-annual work plan 2014-2020," 2014.

[36] The First Group, "Leicester Bus Route Maps." [Online]. Available: https://www.firstgroup.com/leicester/routes-and-maps/route-maps. [Accessed: 31-Jul-2019].

[37] E. McKenna and M. Thomson, "High-resolution stochastic integrated thermal-electrical domestic demand model," *Appl. Energy*, vol. 165, pp. 445–461, 2016.

[38] A. G. Abo-khalil, “Impacts of Wind Farms on Power System Stability. Modeling and Control Aspects of Wind Power Systems,” in *Modeling and Control Aspects of Wind Power Systems*, no. March, IntechOpen, 2013, pp. 133–151.

[39] S. E. George, “United Kingdom Windspeed - Measurement, Climatology, Predictability and Link to Tropical Atlantic Variability,” Benfield Hazard Research Centre - University College London, 2006.

[40] M. L. Kubik, P. J. Coker, and C. Hunt, “Using meteorological wind data to estimate turbine generation output: a sensitivity analysis,” in *World Renewable Energy Congress 2011 - Wind Energy Applications*, 2011, pp. 4074–4081.

[41] A. Lanzini, D. Ferrero, and M. Santarelli, “Energy System Analysis of SOFC Systems,” in *Advances in Medium and High Temperature Solid Oxide Fuel Cell Technology*, vol. 574, 2017, pp. 223–264.

[42] Nord Pool, “N2EX Day Ahead Auction Prices,” 2017. [Online]. Available: https://www.nordpoolgroup.com/Market-data1/GB/Auction-prices/UK/Daily/?view=table. [Accessed: 09-Sep-2018].

[43] Union Internationale des Transport Publics (UITP), “Bus Systems in Europe: Towards a Higher Quality of Urban Life and a Reduction of Pollutants and CO_2 Emissions,” 2015.

[44] Department for Business Energy and Indsutrial Strategy, “2017 government GHG conversion factors for company reporting - Methodology Paper for Emission Factors,” no. August, 2017.

[45] A. Baldinelli, L. Barelli, and G. Bidini, “Progress in renewable power exploitation: reversible solid oxide cells-flywheel hybrid storage systems to enhance flexibility in micro-grids management,” *J. Energy Storage*, vol. 23, no. April, pp. 202–219, 2019.

[46] N. Thambiraj, C. Suciu, I. Waernhus, A. Vik, and A. C. Hoffmann, “Effect of oxygen depletion to the cathode on the working of solid oxide fuel cells,” *ECS Trans.*, vol. 78, no. 1, pp. 875–887, 2017.

[47] J. Larminie and A. Dicks, *Fuel Cell Systems Explained*, 2nd ed. Chippenham (UK): John Wiley & Sons Ltd., 2003.

[48] C. H. Wendel, P. Kazempoor, and R. J. Braun, “A thermodynamic approach for selecting operating conditions in the design of reversible solid oxide cell energy systems,” *J. Power Sources*, vol. 301, no. January, pp. 93–104, 2016.

[49] N. Q. Minh and M. B. Mogensen, “Reversible Solid Oxide Fuel Cell Technology for Green Fuel and Power Production,” *Electrochem. Soc.*, pp. 55–62, 2013.

[50] P. Iora, M. A. A. Taher, P. Chiesa, and N. P. Brandon, “A novel system for the production of pure

hydrogen from natural gas based on solid oxide fuel cell e solid oxide electrolyzer," vol. 5, pp. 1–8, 2010.

[51] L. Eudy, M. Post, and M. Jeffers, "Fuel Cell Buses in U.S. Transit Fleets: current status 2016," NREL/TP-5400-67097, National Renewable Energy Laboratory - Golden, CO 80401, 2016.

SUPPLEMENTARY MATERIAL

A. Steady-state model of the plant

The SOC models implemented in Aspen are based on stoichiometric reactors for the H_2 oxidation (SOFC) and H_2O reduction (SOEC) with separators for dividing anodic and cathodic flows. In SOFC model, the hydrogen and oxygen (21%$_v$ in ambient air) utilizations imposed are equal to 80% and 90%, respectively; in SOEC model, water utilization is 60%. The high level of oxygen utilization in SOFC is due to the minimum air excess imposed. In fact, instead of using cathodic air, the stack thermal management is entirely performed by the heat pipes [25], with 10% of air excess only to avoid excessively low O_2 partial pressure at the cathode. As reported in experimental studies [46], solid oxide cells can operate with such a low air excess without showing relevant performance drops.

Model of the SOFC subsystem

The core of the system (Figure A.1) is represented by the stack, where hydrogen is electrochemically converted into electric power and heat, due to the exothermicity of the redox reaction. The SOFC has been modeled as a stoichiometric reactor combined with a separator. The stoichiometric reactor simulates the oxidation of hydrogen into water occurring at the anode of the fuel cell: it is fed by the fuel flow with an excess index equal to 1.25 [23], [47], [48] and by pre-heated oxidant flow, which passes through the cathode. An air excess of 10% of the stoichiometric value is assumed. It is worth noting that this air excess is needed just to avoid excessively low oxygen partial pressure in the air electrode, and it is significantly lower than in the case of air-cooled SOFCs thanks to the presence of the heat pipes which perform the thermal management of the stack. To account for the separation of fuel and oxidant flows due to the presence of the interposed electrolyte in the real cells, the fictitious product flow exiting the stoichiometric reactor in Aspen-based model enters a separator: in this "dummy" component, the nitrogen and the unreacted oxygen (cathode outlet in the real cell) are separated from the unreacted hydrogen and the water (anode outlet in the real cell). The spent air flow is sent to venting after heat recovery, while the exhaust anodic flow is recirculated to the stack inlet after condensing and separating the water. A small fraction of water remains in the flow to ensure a minimum humidification at the stack anode inlet, representing the 3% of the inlet stream of the anode.

The feeding flows (i.e., air and hydrogen) are preheated to 700 °C before entering the SOFC and the heat produced in the stack is exploited to bring the feeding flows to the stack temperature, which is 800 °C. Having fixed a temperature of 800°C for both SOFC and SOEC operations and being the concentration of chemical species constant, it is possible to compute the value of OCV using Nernst equation:

$$OCV = -\frac{\Delta g_{react}(T, p_0)}{z_F F} + \frac{RT}{z_F F} \ln \frac{\prod_i^{reac} y_i{}^{\nu_i}}{\prod_i^{prod} y_i{}^{\nu_i}} \qquad \text{Eq. (A.1)}$$

where $\Delta g_{react}(T, p_0)$ = 188,691 J/mol is the Gibbs free energy of reaction at p_0 = 1 bar; z_F is the charge number (equal to 2 for hydrogen); F = 96,485 C/mol is Faraday's constant; R = 8.314 J/mol/K is the universal gas constant. The logarithmic term considers the effect of molar fractions of reactants and products, each raised to its stoichiometric coefficient and referred to the inlet of the stack.

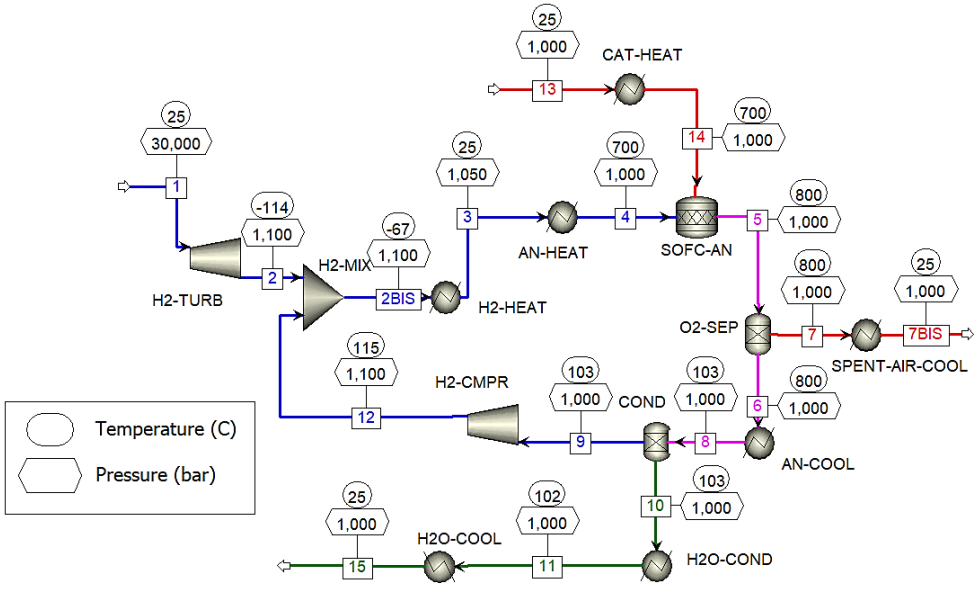

Figure A.1 - Aspen Plus™ flowsheet of the SOFC model

The OCV described in Eq. (A.1) is strictly valid only at zero current. Thus, in order to take into account the water production under current, the molar concentration of water at the outlet has been used in the calculation of the logarithmic term of the OCV used in Eq. (1). The resulting OCV value is 0.95 V.

The nominal operating point of the simulated cell has been chosen by setting a reasonable value of the cell voltage that allows to obtain the maximum power density of the cell. This arbitrary value is set equal to 0.77 V [22], [49], [50] and corresponds to the diffusion overvoltage knee at the end of the linear ohmic region of the polarization curve (current density of 0.77 A/cm^2), over which the stack would work in unfavorable conditions. To obtain the system nominal AC power size of 10 MW_e (assuming a DC/AC inverter efficiency equal to 0.9), a total of about $4*10^4$ cells is thus necessary.

Model of the SOEC subsystem

A similar approach to that used for modelling the SOFC has been used for the reverse operating mode (electrolyzer) (Figure A.2 – top), with attention to the delicate issue of the thermal management: in fact, the cells can work either in endo- or exothermal conditions according to the operating current or voltage.

In general, it is a good practice to work with an excess of reactant. In commercial devices, the reactant utilization ranges between 0.6 and 0.7: the lower bound of this range is chosen in the developed model.

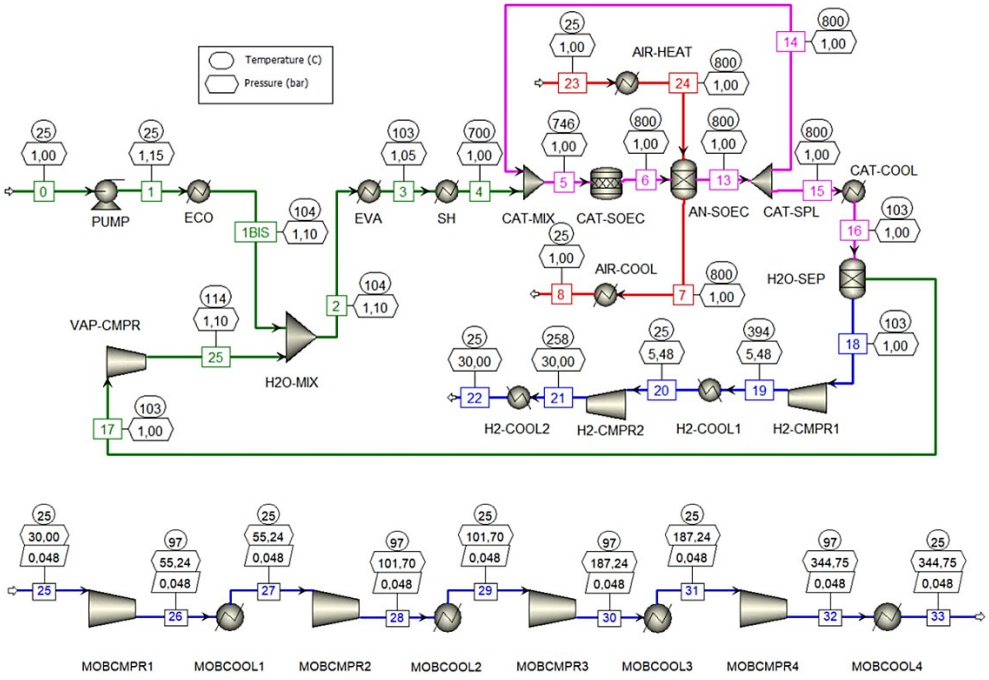

Figure A.2 – (Top) Process flowsheet of the SOEC model and (bottom) of the mobility H_2 compression train

An important issue is the protection of the cathodic nickel from oxidation: to avoid it, especially at higher current density, it is necessary to ensure a reducing environment already at the inlet of the cathode. The cautious solution adopted in the model consists in the partial recirculation of the cathode exhaust rich in hydrogen (almost $10\%_{mol}$ at the cathode inlet in commercial devices). Also in this case, in order to take into account the effect of the current, the outlet concentration of H_2 has been used for the calculation of the OCV used in the polarization equation. Moreover, to ease the downstream calculations, a continuous polarization line between SOFC and SOEC mode has been assumed by determining the recirculation ratio of cathodic product that ensures an OCV of 0.95 V.

The above-mentioned conditions are satisfied in case of 61/39%$_{mol}$ H_2O/H_2 inlet mixture, keeping reactant utilization equal to 0.6. The inlet mixture is fed at 700 °C to the cathode of the stack, as in the SOFC mode. The hydrogen produced at the cathode is separated from the unreacted water and compressed to 30 bar with a two-stage intercooled compression. The water separated is recirculated and mixed with the make-up water in the steam generation section.

To avoid the risk of delamination, i.e., the detachment of the anode layer from the electrolyte one, due to excessively high concentrations of oxygen, preheated sweep air is injected into the anode with a flow rate assumed to be 15%$_{mol}$ of outlet oxygen produced by electrolysis. The sweep air is preheated to 800 °C before entering the stack. At the outlet of the stack, the air enriched with oxygen is cooled and vented.

Once OCV, ASR and the nominal power input of the SOEC are set, then the resulting values for nominal cell voltage and current density are 1.37 V and 1.74 A/cm^2, respectively, which correspond to the operating point that ensures the SOEC/SOFC power ratio of 5 (calculated on the AC power).

Since part of the hydrogen is delivered to the refueling station serving the identified transportation application, an additional model (Figure A.2 – bottom) simulates a 4-stage intercooled post-compression train elevating the pressure of this share of electrolytic hydrogen from 30 bar up to the mobility storage conditions (344.75 bar) [51].

Results of pinch analysis

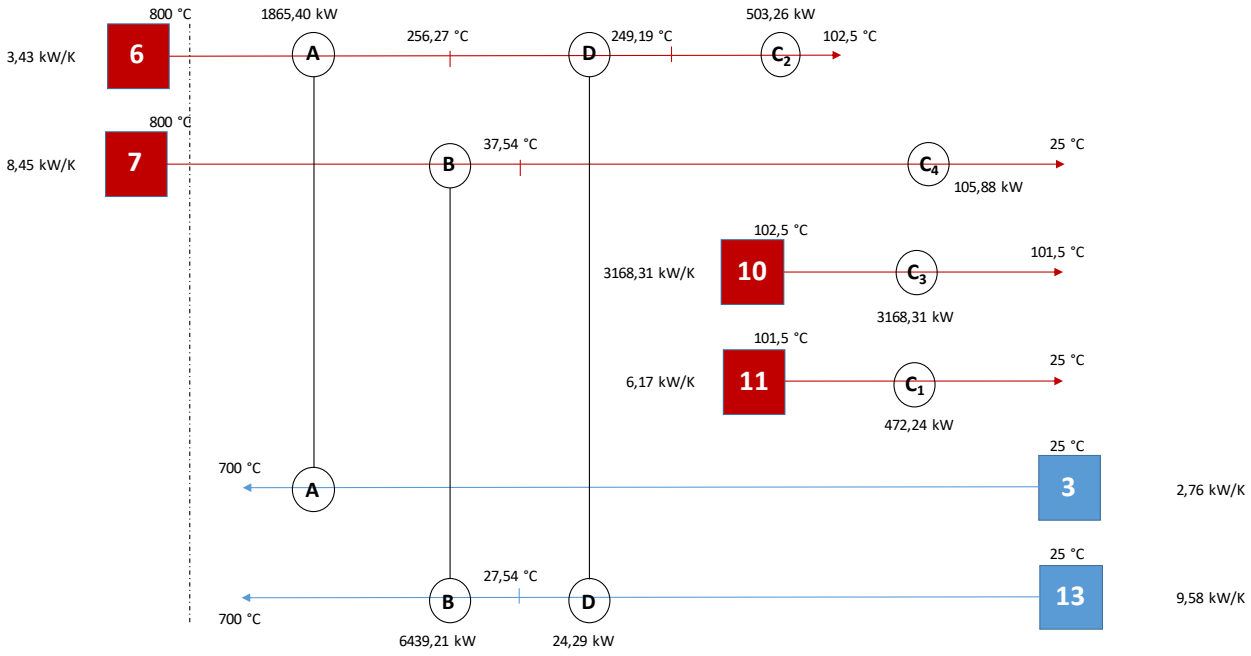

Figure A.3 - Pinch analysis of the SOFC subsystem

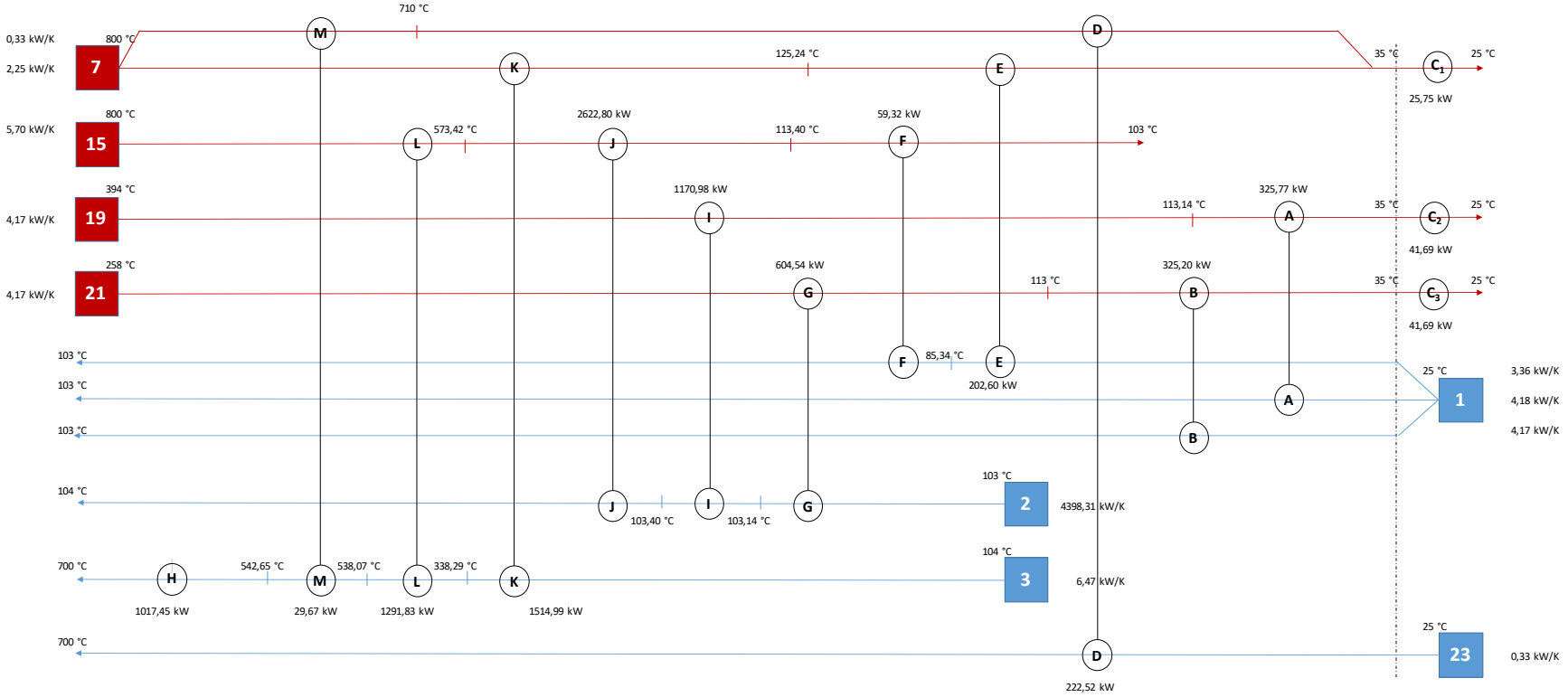

Figure A.4 - Pinch analysis of SOEC subsystem

B. System performance

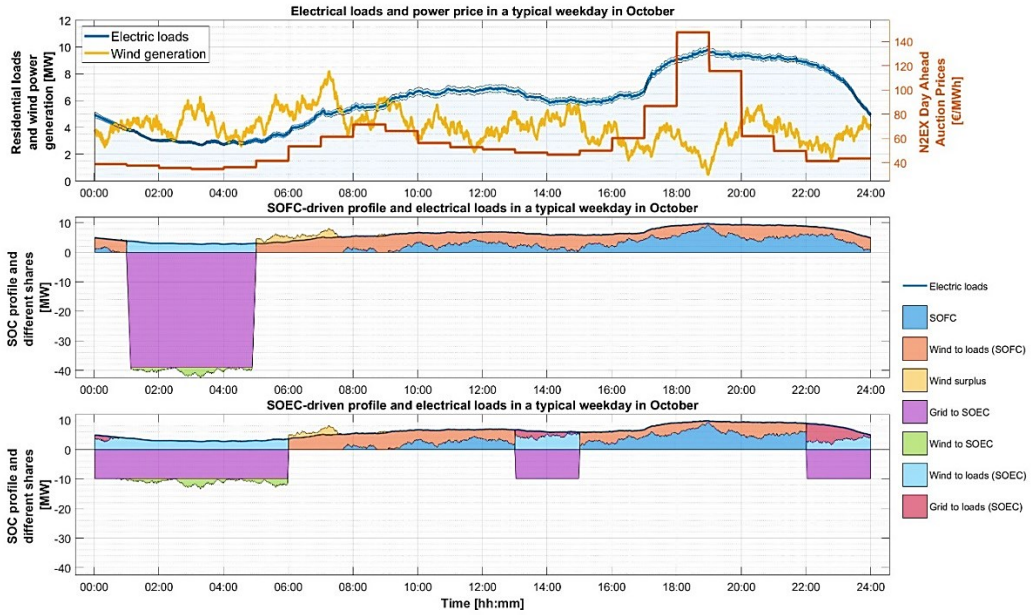

Figure B.1 - Peak of electric demand fulfilled by the grid in case of SOEC-driven strategy (weekdays in October)

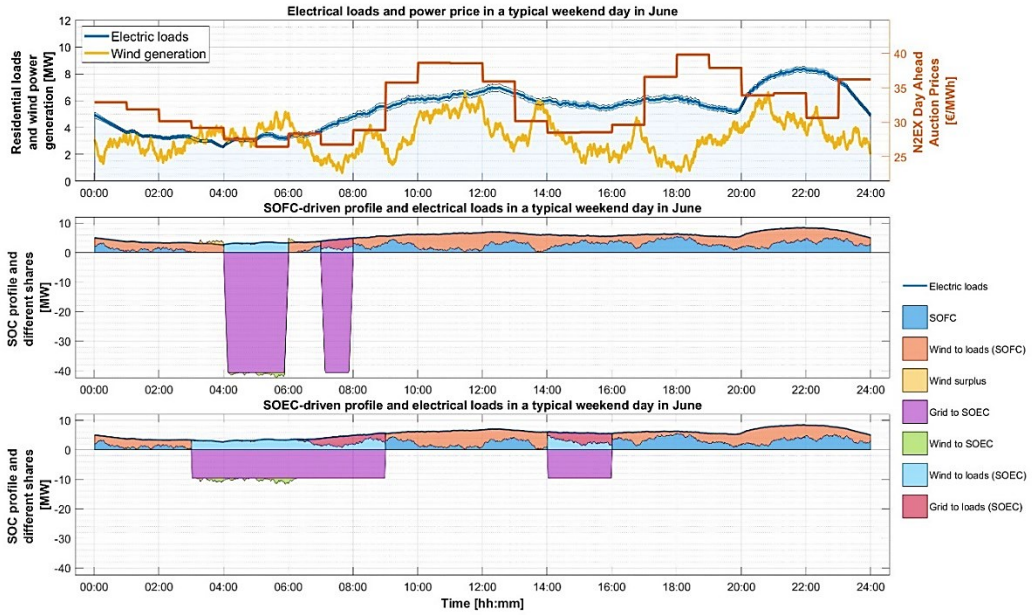

Figure B.2 - Peak of electric demand fulfilled by the grid in case of SOFC-driven strategy (weekend days in June)